

Cyclic and Post-Cycling Anchor Response in Geocell-Reinforced Sand

S.N. Moghaddas Tafreshi^{1,*} (Corresponding Author), M. Rahimi², A.R. Dawson³, B. Leshchinsky⁴

^{1,*}Corresponding Author. Department of Civil Engineering, K.N. Toosi University of Technology, Valiasr St., Mirdamad Cr., Tehran, Iran. Tel: +982188779473; Fax: +982188779476; E-mail address: nas_moghaddas@kntu.ac.ir

²Department of Civil Engineering, K.N. Toosi University of Technology, Valiasr St., Mirdamad Cr., Tehran, Iran. Tel: +982188779473; Fax: +982188779476; E-mail address: my.rahimi@mail.kntu.ac.ir

³Nottingham Transportation Engineering Centre, University of Nottingham, Nottingham, UK. Tel: +441159513902; Fax: +441159513909; E-mail address: andrew.dawson@nottingham.ac.uk

⁴Forest Engineering, Resources and Management Department, College of Forestry, Oregon State University, 280 Peavy Hall, Corvallis, Oregon 97331, USA. Tel: +1541-737-8873; E-mail address: ben.leshchinsky@oregonstate.edu

33 **Abstract:**

34 Plate anchors are commonly used to resist static, cyclic and monotonic after cyclic-loading uplift loads. Under
35 cyclic loading, progressive sudden failure may occur, characterized by accumulated displacement – even under loads
36 significantly less than the static capacity. Despite extensive usage of geocell for increasing the cyclic resilience, the
37 influence of geocell reinforcements on cyclic uplift capacity is not well-understood. In this study, a series of near-full
38 scale, experimental tests with and without geocell are presented. Results show that the unreinforced system fails
39 cyclically under a load that is almost 70% of its static capacity (P_u), but use of geocell enables stable cyclic resistance
40 of over $100\%P_u$. For the given soil and configurations, a cyclic displacement rate that reaches less than 0.05 mm/cycle
41 tends to highlight a likely stable response. Evaluation of the soil's response to cyclic loading demonstrates that, with
42 increasing loading cycles, the loading is increasingly transmitted through the soil close to the anchor in the
43 unreinforced case, but that the reinforced case is less prone to this phenomenon. The monotonic post-cycling capacity
44 of both reinforced and unreinforced anchors decreases after application of cyclic loading; however, the unreinforced
45 scenario demonstrates larger decreases in capacity, particularly in the residual capacity.

46

47 **Keywords:** *Anchor, Uplift, Geocell, Cyclic Loading, Post-cycling Behavior, Large-Scale Testing*

48

49

50

51

52

53

54

55

56

57

58

59

60

61

62 1. Introduction

63 The stability of various structures (e.g. masts, wind turbines, rock-fall protection fences, etc.) may directly depend
64 on anchoring that may resist static and cyclic uplift loadings. Under cyclic uplift loading of anchoring systems,
65 cumulative displacements may occur, resulting in the onset of failure over time ([Andreadis and Harvey, 1981](#);
66 [Schiavon et al., 2017](#)). The onset of progressive anchoring failure is often a function of the magnitude of static and
67 cyclic loading, soil type, and anchoring system. Hence, the primary design requirement for many anchoring systems
68 is to obtain sufficient resistance to static and cyclic load while keeping the cyclic displacement behavior compatible
69 with structural mooring requirements. Thus, it is accepted that both ultimate and service limit states be considered in
70 the design of anchoring. Due to the complexity of soil behavior under repeated loading, the design of anchors under
71 cyclic loading is generally conservative – reliant on a high factor of safety applied to the static load capacity. However,
72 design for static conditions may still neglect potential instability due to progressive anchor displacement. Hence, it is
73 critical to arrest cumulative cyclic anchor displacements to sustain both short-term and long-term stability. One viable
74 means of mitigating progressive deformation of soil under cyclic loading is the application of geosynthetic
75 reinforcement. Although commonly used to inhibit cyclic deformation and “ratcheting” under compressive loading
76 ([Mengelt et al., 2006](#); [Indraratna et al., 2014](#); [Ngo et al., 2015](#); [Basack et al. 2015](#); [Thakur et al., 2016](#); [Suku et al.](#)
77 [2016](#), [Koshi and Unnikrishnan, 2016](#); [Satyal et al., 2018](#); [Kargar and Hosseini, 2018](#); [Dash and Choudhary, 2018](#) and
78 [Wang et al. 2018](#)), the application of geosynthetics are promising for resisting uplift loads as well. Of particular
79 promise are three-dimensional (3D) geocells reinforcements ([Koerner, 1998](#)), which provide three mechanisms of
80 lateral resistance effect, vertical stress dispersion and membrane mechanism for increasing the load bearing capacity
81 and improving the performance of pavement ([Koerner, 1998](#); [Zhang et al., 2010](#); [Sitharam and Hegde, 2013](#); [Hegde,](#)
82 [2017](#)).

83 The cyclic uplift behavior of anchors is complex, and often a function of soil, anchor dimensions, loading
84 magnitude, and loading pattern. [Ponniah and Finlay \(1988\)](#), [Datta et al.\(1990\)](#), [Prasad and Rao \(1994\)](#), [Singh and](#)
85 [Ramaswamy \(2008, 2010\)](#) and [Yu et. al. \(2015\)](#) used scaled experiments to observe the cyclic behavior of plate
86 anchors in cohesive soils, observing that anchor systems may exhibit different cyclic response based on soil
87 compressibility, shear strength, and embedment. Similar observations were made about cyclic uplift behavior being
88 influenced by embedment, cyclic loading pattern and relative density in granular materials ([Andreadis and Harvey,](#)

89 1979, 1981; Petereit, 1987; Byrne 2000; Choudhury and Subba Rao, 2005; Wang and O’Loughlin, 2014; Schiavon
90 2016; Stuyts et al. 2016; Schiavon et al., 2017 and Pérez et al., 2018).

91 However, there is limited research focusing on the beneficial role that geosynthetics may play in enhancing cyclic
92 resistance of anchoring systems. Ravichandran et. al. (2008) studied the behavior of plate anchors buried in geogrid-
93 reinforced sand under monotonic and repeated loading – for the limited set of tests, it was observed that the
94 geosynthetic systems helped increase uplift capacity. Moghaddas Tafreshi et al. (2014a) investigated the influence of
95 geocell reinforcement on improving cyclic uplift resistance of belled piles, demonstrating significant improvement
96 when the reinforcement was present. However, the available studies are either limited in scale or in breadth of design
97 factors considered.

98 The objective of this study is to better assess the role of geosynthetics reinforcement in the vertical cyclic uplift
99 load response and in the monotonic load response after a period of cyclic loading (the ‘post-cycling’ uplift behavior)
100 of plate anchors, particularly when using geocell reinforcement. To achieve this, a series of near full-scale physical
101 tests (a total of 27 independent tests plus extra repeated tests) were performed on a horizontal square plate anchor
102 installed in unreinforced and geocell-reinforced soil. During testing, the load – displacement behavior of geocell-
103 reinforced system was compared to an unreinforced control scenario. The influence of embedment depth and cyclic
104 load amplitude (P_c) on the plate anchor’s uplift response was observed.

105 **2. Materials and Experimental Setup**

106 **2.1. Soil Properties**

107 A well-graded sand (SW, ASTM D2487-11) with specific gravity of 2.66 ($G_s=2.66$) was used to fill the geocell
108 pockets and backfill soil in the testing program. There is a significant quantity of fine gravel (46%) and little fines
109 (<1%), as shown in the grain size distribution (Fig. 1). Based on the modified proctor compaction (ASTM D1557-
110 12), the maximum dry density and optimum moisture content of this soil were approximately 20.42 kN/m³ and 5.1%,
111 respectively. The angle of internal friction (ϕ) of the soil, obtained from consolidated drained triaxial compression
112 tests was 40.5° at a moist density of 19.73 kN/m³ (corresponding to relative compaction of 92%, similar to the
113 compacted density of the backfill soil layers in test pit) and a moisture content of 5%. As the test pit material was

114 partially saturated, suction stresses were present, but were considered negligible for the material used (0.1-1kPa for
115 gravelly sand, Fredlund 2006).

116 **2.2. Geocell Properties**

117 Each cell in the geocell used is 110 mm long and wide (d) and 100 mm high (h). **Fig. 2** shows an isometric view
118 of the geocell spread over the bottom soil layer and the plate anchor. This geocell was manufactured from a nonwoven
119 polymeric geotextile that was thermo-welded without internal perforations within each pocket. The engineering
120 properties of this geotextile, as listed by the manufacturer, are presented in **Table 1**. In all tests, the ratio of the geocell
121 pocket size (d) to width of anchor plate ($B=300$ mm) were kept constant. However, the d/B ratio adopted is not
122 necessarily the optimum value and a change in this ratio might increase or decrease the resistance encountered. Future
123 research could investigate optimal dimensions of geocell anchoring.

124 **2.3. Experimental Setup**

125 To investigate the uplift capacity and upward displacement of plate anchors supported by geocell layers, large-
126 scale testing on a square steel anchor plate with width of 300 mm and 2.54 mm thickness attached to an anchor rod
127 with diameter of 50 mm was conducted in an indoor test pit. The test pit, measuring 2200 mm \times 2200 mm in plan and
128 1000 mm in depth, contained the soil, anchor, geocell reinforcement and instrumentation (i.e. load cell, LVDTs and
129 pressure cells). The four sides of the test pit were vertical (**Fig. 3**). Because the width and depth of the test pit were
130 respectively more than seven and three times bigger than the width of the anchor, the boundary effects during testing
131 were not considered to be significant ([Consoli et al., 2012](#)).

132 The loading system (**Fig.3**) consisted of a loading frame, hydraulic actuator, and a controlling unit. The loading
133 frame is comprised of two heavy steel columns fixed in the ground and a horizontal strong reaction beam spanning
134 the width of the test pit that supports a hydraulic actuator. The hydraulic actuator and control unit may produce
135 monotonic or cyclic loads with the capability of applying a stepwise controlled load with a maximum tensile capacity
136 of 100 kN. The loading frequency of the loading system was in the range of 0.05 Hz to 0.5 Hz, but the best performance
137 was at the 0.1 Hz which is desirable to simulate the low frequency of the wind loads ([Herrmann, 1981](#); [Rao and Prasad,](#)
138 [1991](#); [Singh and Ramaswamy, 2008](#)).

139 A custom data acquisition system was developed to read and record applied uplift loading, displacements and soil
140 pressures at a frequency of 100 Hz. A load cell with the accuracy of $\pm 0.01\%$ and a full-scale capacity of 100 kN was

141 placed between the loading shaft and a rod attached to the plate anchor (**Fig. 3a**). To measure the displacement of the
142 plate anchor during the loading, a Linear Variable Differential Transducer (*LVDT*) with the accuracy of 0.01% of full
143 range (100 mm) was attached to the loading shaft and the supporting beam (as shown in **Fig. 3**). In some tests, two
144 soil pressure cells (“SPC”) monitored the soil pressure at a depth of 100mm above the anchor (the depth of the upper
145 edge of the geocell) (**Fig. 3b**). The pressure cells had a capacity of 1000 kPa and an accuracy of 0.01% (0.1kPa), small
146 enough to not significantly influence measurements. To prevent stress concentrations from asperities on soil grains
147 located adjacent to the pressure cell, each cell was placed in a small bag filled with clay for consistent transferring of
148 stress to the pressure cells. The suffixes “i” and “o” are used to indicate the inner and outer positions 50 and 150 mm
149 away from the center of anchor, respectively. All output data streams (load cell, LVDT and pressure cells) were
150 recorded continuously using a data acquisition system within internal processor. To ensure an accurate reading, all of
151 the devices were calibrated prior to each test series. **Fig. 3a** illustrates the test installation prior to loading. A schematic
152 cross-section of the experimental set-up containing the test pit, loading system and data measurement system, geocell
153 layer, and the anchor is shown in **Fig. 3b**.

154 **2.4. Preparation of Test Pit and Experimental Procedure**

155 In order to compact the unreinforced layers and geocell-reinforced layer in the test pit (**Fig. 3**), a handheld
156 vibrating plate compactor was used. In all the tests, depending on the embedment depth of anchor the unreinforced
157 soil layers were prepared and compacted at thicknesses of either 50 or 100 mm with respectively one or three passes
158 of the compactor to achieve the required density (i.e. dry density of $\approx 18.78 \text{ kN/m}^3$ in **Table 2**). As the same the soil
159 filled the pockets of geocell layer was compacted with four passes of compactor to achieve the required density of soil
160 layer (shown in **Table 2**). This amount of compactive effort was maintained throughout the testing series. The density
161 of the both unreinforced and reinforced layers were checked for compaction specifications through sand cone testing
162 (**ASTM D1556-07**), performed at least three times per lift. A maximum difference of approximately 1-2% was
163 observed between the measured and desired density of compacted layer. The materials used were compacted at an
164 optimum moisture content of 5%, but the average measured (recovered) moisture content of the layers was between
165 4.8% and 5.2%. The exposed backfill material was covered with a waterproof paper to limit possible moisture loss.

166 To prepare the backfill in the test pit, a 100 mm thick unreinforced soil layer was compacted first. Then, the
167 anchor plate was placed in the center of the test pit on the surface of compacted soil layer, with the correct connected

168 length of the rod. Thereafter, the geocell reinforcement (in the reinforced case) was spread above the anchor and cell
169 pockets were filled and compacted (dry density of 18.2-18.4 kN/m³) with backfill soil with about 10 mm extra
170 thickness of soil over the geocell. Two soil pressure cells were then installed. The desired level of the soil
171 surface/embedment depth was achieved, after the compaction of unreinforced soil layers above the geocell layer
172 (average dry density of 18.78 kN/m³). When the installation was prepared for testing, a desired loading pattern
173 including initial monotonic and subsequent cyclic load (see section 2.5.) was applied to the anchor plate, while upward
174 displacement, uplift force and soil pressure were recorded using the aforementioned LVDT, load cell and soil pressure
175 cells (SPCi and SPCo), respectively.

176

177 **2.5. Experimental Series and Loading Pattern**

178 Increased embedment depth of anchors results in enhanced anchor capacity. Therefore, three embedment depth
179 ratios ($D/B=1.5, 2, 2.5$) were assessed for both unreinforced and geocell-reinforced backfills under monotonic and
180 cyclic loading. The geocell width in all the monotonic and cyclic reinforced tests was selected to be three times the
181 width of the geocell layer ($b/B=3$ or $b=900$ mm) since the influence of more extensive soil reinforcement on uplift
182 capacity decreases outside this range (Choudhary and Dash, 2013; Rahimi et al., 2018a). The thickness of the geocell
183 layer above the anchor plate was held constant in all tests at 100 mm. The details of the test program are given in
184 **Table 3**. Six monotonic uplift tests (series 1-2) at three embedment depth ratios ($D/B=1.5, 2, 2.5$) were conducted to
185 obtain the ultimate uplift resistance of unreinforced (P_u) and reinforced (P_r) beds, respectively. Monotonic loading
186 was continued until softening behavior had occurred in the load-displacement response or the maximum stroke of the
187 actuator (20 mm) had been reached. The monotonic ultimate uplift capacity obtained from Test Series 1 and 2 are
188 used to compare with post-cycling uplift capacity (see Section 3.7.). Furthermore, the unreinforced capacity (P_u)
189 determined in testing (Test Series 1) was then used to determine cyclic load ratios in Test Series 3 (cyclic loading,
190 unreinforced) and Test Series 4 (cyclic loading, geocell-reinforced). Another object of Test Series 3 and 4 is
191 determination of the anchor's post-cycling uplift resistance.

192 Typically, anchors endure sustained loads, but additional cyclic loading may occur in addition to static loading
193 (e.g. winds, wave loading, and vibrations), which may influence anchor performance for a short time period.
194 Furthermore, anchor serviceability under monotonic post-cycling loading after cyclic load application may have great

195 importance. Therefore, the loading pattern for cyclically-loaded tests were divided into three phases as shown in **Fig.**
196 **4**:

197 i) *Monotonic loading*: The ratio of applied initial sustained load (P_s) to monotonic ultimate uplift capacity
198 of unreinforced installation (P_u) is expressed as $SLR=P_s/P_u$. A fixed and constant SLR value of 30%
199 ($SLR=P_s/P_u=0.3$) was applied for each respective embedment depth, as the typical factor of safety for
200 design is approximately three. In all the tests, the initial sustained load (P_s) was applied with a rate of 1.5
201 kPa per second to the both unreinforced and reinforced system (**Fig. 4**). After reaching the predefined P_s ,
202 the load is kept constant for approximately 120 seconds as to stabilize anchor movement before applying
203 cyclic loading. To control the rate of 1.5 kPa per second (i.e. the rate of 0.135 kN per second) during
204 monotonic loading, the predefined P_s was applied at a fixed duration which was operated by an automated
205 load control system.

206 ii) *Cyclic loading*: After the sustained load is reached, 250 sinusoidal loading cycles of amplitude P_c and 10
207 $sec.$ period (0.1 Hz frequency) are applied to the anchor (**Fig. 4**). Typically, the actual frequency of wind
208 load, simulated herein, is no greater than 0.1 Hz (Herrmann, 1981). A 10 $sec.$ period has been commonly
209 applied in the physical modeling of cyclically-loaded anchor plates which are exposed to the low
210 frequency loads of the wind storms (Ponniah and Finlay, 1988; Rao and Prasad, 1991; Singh and
211 Ramaswamy, 2008). For each cycle of loading and unloading, the load in the anchor was varied from
212 sustained load (P_s) to the desired cyclic load (P_s+P_c), where (P_c) was amplitude of cyclic loading (**Fig.**
213 **4**). Three cyclic load ratios ($CLR=P_c/P_u=20, 30$ and 40%) were assessed for unreinforced conditions and
214 four cyclic load ratios ($CLR=40, 50, 60$ and 70%) were assessed for reinforced conditions. It is worth
215 noting that 30% of the static uplift capacity of the reinforced system is greater than the corresponding
216 value for the unreinforced case, thus, a higher CLR was selected for cyclic loading under reinforced
217 conditions as to bring the anchoring system closer to failure. However, a CLR of 40% was presented for
218 both reinforced and unreinforced systems for direct comparison. Cyclic loading was continued until 250
219 loading cycles were completed, when 20 mm of uplift had reached, or cyclic failure occurred. For this
220 preliminary study, 250 loading cycles deemed reasonable to assess general anchor behavior as this range
221 exhibited displacement accumulation rates that were small enough for low amplitude loading ($CLR<40\%$)

222 and large for high amplitude cyclic loading ($CLR \geq 40\%$), which is often short in duration for well-
223 designed anchor systems (Schiavon et al., 2017).

224 iii) *Post-cycling loading*: If cyclic failure had not occurred after the completion of 250 loading cycles, a
225 monotonic load was applied once more at a rate of 1.5 kPa per second to evaluate the post-cycling
226 capacity of plate anchor.

227 Several replicate installations were performed to confirm the repeatability of the loading behavior, instrumentation
228 and loading control. The results obtained showed a close match between results of the repeated tests: the maximum
229 difference between the results was about 6-8%, so the results were considered reliable.

230

231 3. Results

232 In this section, the results of the monotonic and cyclic uplift tests are presented for varying embedment, cyclic
233 loading amplitude (CLR), and reinforcement conditions. Cyclic uplift displacement, rate of anchor displacement, soil
234 pressure above the anchor (in a few tests- Section 3.6) and post cycling uplift capacity of anchor plate were evaluated.

235 3.1. Ultimate Capacity of Reinforced and Unreinforced Anchors under Monotonic Loading

236 To define the sustained load ratio (SLR) and cyclic load ratio (CLR) to be used in the subsequent cyclic loading
237 tests, the ultimate uplift capacity was determined in six monotonic uplift tests performed at three different embedment
238 depth ($D/B=1.5, 2.0$ and 2.5) for unreinforced and geocell-reinforced conditions. Fig. 5 shows the load-displacement
239 behavior of unreinforced and reinforced cases at different embedment depth ratios. In general, the uplift load-
240 displacement response demonstrated for unreinforced conditions was characterized by a relatively rapid increase in
241 loading until a peak was reached, followed by a distinct softening behavior with continued displacement. For geocell-
242 reinforced conditions, peak resistance was sustained over a range of upward displacement with no distinct softening
243 behavior occurring for the given range of displacement evaluated in the tests. In both cases, the inferred peak loads
244 for the unreinforced case was used to determine P_s . More details about static results are available in Rahimi et al.,
245 (2018b).

246

247 3.2. Overall Cyclic Behavior of Unreinforced and Geocell Reinforced Anchor Systems

248 Both the unreinforced and reinforced installations were tested with a fixed static load ratio ($SLR=30\%$) and varying
249 cyclic load ratios (CLR) as shown in **Table 3**. Two general types of load-displacement behavior were observed under
250 the application of loading cycles, characterized as behavior (1) where no failure occurs under cumulative cyclic
251 displacement (*stable* condition), or (2) where a certain CLR may result in the eventual failure under large cumulative
252 displacement (*unstable* condition).

253 *Stable* conditions were observed for lower cyclic loading magnitudes ($CLR \leq 30\%$) in unreinforced conditions and
254 for all reinforced scenarios (except for $D/B=1.5$ with $CLR=70\%$). An example of typical cyclic behavior under *stable*
255 conditions is presented in **Fig. 6a** for first 1500 *sec.* of loading. This figure shows that at the first phase of loading
256 (monotonic loading) anchor displacement increases linearly with time. After initial monotonic loading, anchor
257 displacement increases nonlinearly under the application of cyclic loading, reducing with each loading cycle and even
258 reaching a relatively stable state where displacements are primarily elastic. This characteristic may be defined as
259 “plastic shakedown” (Werkmeister et al., 2007), whereas stress states that are less than that required for progressive
260 failure result in long-term, steady-state response where no collapse is observed. **Fig. 6b** shows the load hysteresis
261 derived from the same test. In most of the tests, a large proportion of total anchor uplift displacement (between 15%
262 to 55% of total displacement) occurs in the first cycle, reaching an eventual stable state under applied cyclic loading.
263 With increased load cycles, the hysteresis loops become more symmetric and loading and unloading paths become
264 closer, implying that the load-displacement response is acting under increasingly elastic conditions.

265 *Unstable* behavior was observed for unreinforced conditions when CLR was greater than 40% and for geocell
266 reinforced conditions when $CLR=70\%$ at embedment depth of $D/B=1.5$ as shown typically in **Fig. 6c-d**. For
267 unreinforced conditions, the *stable* trend of reduced anchor upward displacement was sustained unless a cyclic load
268 ratio exceeded a critical magnitude that led to eventual cumulative displacement and catastrophic failure, defined as
269 the critical cyclic load ratio (CLR_{cr}). Thus in the unreinforced system, all the tests performed with $SLR=30\%$ and CLR
270 less than 40% of the monotonic uplift capacity delivers a stable response, but when CLR exceeds 40% ($CLR_{cr}=40\%$),
271 the unreinforced system is no longer stable under the applied cyclic load, exhibiting cumulative plastic, cyclic
272 displacements. Use of reinforcement may attenuate some of the progressive displacements that occur under cyclic
273 loading. The reinforced system can distribute load to a wider area and prevent shear localization, consequently

274 inhibiting strain localizations and progressive failure mechanisms. Fig. 6c-d shows typical unstable behavior under
275 cyclic loading. As seen in Fig. 6c, displacements continue to increase with loading cycles, ultimately realizing a
276 catastrophic failure after definite cycles of loading. Fig. 6d shows the load-displacement hysteresis of the *unstable*
277 behavior. With increasing load cycles, the system cannot maintain the desired load level, gradually reaching failure
278 conditions where permanent displacements increase with each loading cycle.

279 3.3. Cyclic Loading of Unreinforced Anchors

280 Fig. 7 shows the cumulative displacements measured at the peak of each loading cycle for unreinforced
281 conditions under cyclic load ratios of $CLR=20\%$, 30% and 40% at D/B of 1.5, 2 and 2.5 and Fig. 8 shows the
282 displacement accumulation rate during cyclic loading. As cyclic load ratio increases, cumulative displacement
283 increases either for all embedment depths, although the rate of increase of displacement is higher for more shallowly-
284 embedded anchors (e.g. $D/B=1.5$). As CLR exceeds 40% , the system fails progressively under cumulative
285 displacement. Thus $CLR=40\%$ is a critical cyclic load amplitude that is the threshold between a stable and unstable
286 response of the unreinforced bed. As the embedment depth increases, the number of loading cycles required to reach
287 to the critical cyclic load ratio increase commensurately. For example, the number of cycles to failure for CLR of 40%
288 and D/B of 1.5, 2.0 and 2.5 was 31, 72 and 148 number of cycles, respectively. However, failure may occur with a
289 different number of loading cycles between CLR of 30% and 40% , but would exceed the cycles required for failure
290 for $CLR=40\%$.

291 As expected, an increase in the amplitude of cyclic load (CLR) causes the progressive anchor displacement to
292 increase. For example, the anchor displacement for the unreinforced bed with embedment depth ratio, $D/B=1.5$, at the
293 end of the cyclic loading are 1.90 and 2.89 mm for the cyclic load with $CLR=20\%$ and 30% , respectively. However,
294 anchor displacement under cyclic loading is greater for smaller embedment depths. As the embedment depth increases,
295 shakedown occurs more rapidly and the maximum displacement at the end of cyclic loading decreases. For example,
296 as the embedment depth increases from $D/B=1.5$ to 2.5, the maximum displacement decreases from 1.90 to 0.77 mm
297 and 2.89 to 1.44 mm for $CLR=20\%$ and 30% , respectively. This behavior may be attributed to the increased stiffness
298 due to the greater confining stress and probably extension of shear zone provided by the increased overburden. When
299 a non-stabilizing response is observed as a consequence of excessive displacement, significant heave at the surface

300 may be observed. This mechanism suggests that the unreinforced soil, when subjected to cyclic loading may eventually
301 fail after excessive displacements occur in the soil around and above the anchor.

302 **Fig. 8** shows the cumulative displacements rate with the number of load cycles for unreinforced conditions
303 under cyclic load ratios of $CLR=20\%$, 30% and 40% at D/B of 1.5, 2 and 2.5. This figure indicates that for $CLR=20\%$
304 and 30% , the displacement accumulation rate decreases rapidly after the first 10 loading cycles, reaching a small and
305 relatively constant value. This rate increases with loading amplitude. Accumulated displacement rate is about to 0.05
306 mm/cycle for $CLR=20\%$ and 30% after 10 loading cycles, but it is always more than 0.05 mm/cycle for $CLR=40\%$
307 and, after some cycles of loading, the displacement accumulation rate begins to rise rapidly and stabilization does not
308 occur. As one might expect, the lower the rate of cyclic displacement after initial shakedown, the more likely that
309 stable cyclic behavior will be sustained throughout cyclic loading as obtained for $CLR=20\%$ and 30% . Schiavon
310 (2016) reported the same trend about helical piles under cyclic uplift load, for which a displacement accumulation rate
311 of less than 0.1 mm/cycles was a sign of stable behavior.

312

313 **3.4. Comparison of Cyclic Response of Unreinforced and Geocell-Reinforced Anchors**

314 As observed for unreinforced conditions, a threshold cyclic load ratio may demonstrate a transition from a stable to
315 an unstable condition – use of soil reinforcement may mitigate this phenomenon. **Fig. 9** compares the behavior for
316 unreinforced and reinforced conditions for $CLR=40\%$. Unlike the unreinforced case, the reinforced case shows a
317 stable response for $CLR=40\%$. As seen in **Fig. 9a**, the cumulative displacements for the reinforced installation is
318 well below the corresponding value in unreinforced condition at same cyclic load ratio. The hysteresis loops for the
319 anchor, shown in **Fig. 9b**, are derived from the unreinforced and reinforced tests. The hysteresis loop of the
320 unreinforced installation shows excessive deformation and subsequently unstable behaviour whereas, in the geocell-
321 reinforced installation, a steady response condition was achieved with the load-displacement path forming a closed
322 hysteresis loop.

323 **Fig. 10a** shows the variation of unreinforced and reinforced displacements for $CLR=40\%$ for three different
324 embedment depth ratios. As seen, in all cases the reinforced installation exhibits a well stabilized response compared
325 with the non-stabilized response of the unreinforced case. The effect of soil reinforcement is that it enables a stable
326 response under cyclic loading as the confined, stiff behavior of the reinforced composite diminishes the upward

327 displacement through mobilization of the reinforcement's tensile resistance and a greater distribution of uplift stresses.
328 **Fig. 10b** shows the displacement accumulation rate for unreinforced and reinforced tests; the rate is well below 0.05
329 mm/cycle after first 10 loading cycles for the reinforced case, a sign of stabilized response, whereas the unreinforced
330 installation all develop instability – taking more cycles for a greater embedment.

331 **Fig. 11** shows the surface heave at the end of cyclic loading with CLR=40% for unreinforced and reinforced
332 beds. As seen in **Fig. 11a**, with application of cyclic load to the unreinforced bed, the soil located above the anchor
333 locally displaced upward and cracks propagated through the soil, leading to a reduction of soil resistance and finally
334 to failure of soil-anchor system. On the other hand as seen in **Fig. 11b** the embedded geocell prevents local
335 displacement of soil and cracks are not observed on the soil surface. In this case, a wider mass of soil was evenly
336 displaced upward, without localized shear displacement. Thus, the combined soil-geocell exhibits a greater
337 resistance against cyclic loading and has limited upward displacement. **Fig. 12** compares the measured surface heave
338 heights at the end of the cyclic loading. These are measured at failure in the unreinforced case (20 mm anchor
339 displacement) and the response after loading cycle number 250 for the reinforced case (failure has not occurred). As
340 seen, in the unreinforced case the anchor causes surface displacements close to the centerline whereas, in the
341 reinforced case, a wider region of soil is displaced. The increased width of the area of surface heave for reinforced
342 versus unreinforced conditions is suggestive of a change in the geometry of the shear failure mechanism.
343 Unfortunately, the actual shape of the failure geometry was not explicitly observed or measured in these
344 experiments. Future work could better describe this mechanism, best captured through numerical modeling. Even
345 though the maximum unreinforced centerline heave is around 7 times greater than in the reinforced case, at a radial
346 distance of 30-35mm (~twice the anchor plate radius) the surface heave is the same. Thus, the geocell layer acts to
347 prevent upward 'punching' failure.

348

349 **3.5. Response of Geocell-Reinforced Anchors under Heavy Cyclic Load**

350 In order to evaluate the reinforced bed's performance under higher cyclic loading, additional tests were performed
351 under cyclic load ratios of *CLR* of 50%, 60% and 70% for *D/B* of 1.5, 2.0 and 2.5. **Fig. 13** shows the load-displacement
352 hysteretic behavior for different cyclic load ratios at *D/B* of 2.0. Increasing the cyclic load ratio results in greater
353 magnitudes of cumulative displacement. Measured displacements after 250 loading cycles were 4.15, 5.02 and 9.84

354 mm for CLR=50%, 60% and 70%, respectively. There is, thus, non-linearity in the deformation response to loading
355 suggesting that punching failure might occur at very large cyclic load ratios (CLRs).

356 **Fig. 14** illustrated the load displacement loop at load cycles of 1, 10, 100 and 200 for the different cyclic load
357 ratios and D/B of 2.0. The plastic displacement at the end of first cycle is much larger than subsequent cycles, meaning
358 that the system's response is stabilizing even at these high loads. The load displacement hysteresis of later cycles tend
359 to approach a constant hysteretical shape that is closed, implying that the load-displacement response is largely elastic
360 (although at a somewhat reduced modulus value by the end of cycling in the CLR=70% case). Modulus is also seen
361 to reduce as CLR increases, indicating a likely transition with some of the load that was carried by the overburden soil
362 now being carried by the geocell reinforcement.

363 **Fig. 15** shows the variation of the uplift displacement of anchor buried in geocell-reinforced bed with cyclic
364 loading for CLR=50%, 60% and 70% at different embedment depth ratios. The reinforced system may sustain large
365 cyclic loading without reaching an unstable state with the exception of shallow anchor embedment, $D/B=1.5$, where
366 the anchor displacement reached the maximum actuator stroke of 20 mm after 57 load cycles. One important advantage
367 of the reinforced system over the unreinforced system is that the reinforced system be able to accommodate a cyclic
368 load representative of the ultimate monotonic uplift capacity of the unreinforced system (e.g. $CLR=70%$ or
369 $P_s+P_c=100\%P_u$) without the loss of function. In this case, the cyclic portion of the load pattern is double the sustained
370 static load (e.g. $P_c>2P_s$), implying that a reinforced system could easily resist heavy cyclic loading. This behavior
371 likely owes to the slab-like behavior of the geocell-soil composite, effectively distributing uplift loading more
372 effectively and mobilizing tensile resistance within the reinforcement structure. Because of the three-dimensional
373 structure of the geocell, the confined cells of soil displace laterally after application of uplift loading, increasing the
374 shear strength of the composite system (Moghaddas Tafreshi and Dawson, 2010; Thakur et al., 2012; 2016; Rahimi
375 et al., 2018a). The confined soil-geocell structure has relatively high flexural stiffness to resist out-of-plane loads.
376 Therefore, the load distribution area increases and upward displacement diminishes, which helps the overall stability
377 of composite layer against static and cyclic loads.

378 **Fig. 16** shows the displacement accumulation rate for different cyclic loads and embedment depth ratios. As
379 discussed before, the displacement accumulation rate in the initial cycles (especially in first 10 cycles) is an important
380 surrogate for describing the long-term stability of anchor cyclic behavior. As seen in **Fig. 16**, as cyclic load ratio

381 increases, the rate of upward displacement increases too. However, after the first 10 cycles (except $D/B=1.5$ and
382 $CLR=70\%$) it decreases rapidly beneath a rate of 0.05 mm/cycle, which as seen in previous sections leading to a stable
383 response for the given soil type and anchor dimensions. Schiavon (2016) reported the same finding for helical piles
384 under cyclic uplift load. Furthermore, after 250 load cycles, the rate of upward displacement decreases to less than
385 0.01 mm/cycle (except $D/B=1.5$ at $CLR=70\%$), implying stability in the short term for cyclic loading and adequacy of
386 250 load cycles for recognition of anchor behavior type (whether stable or unstable behavior). It is observed that the
387 reinforced system tends to experience large displacement prior to reaching a distinct yield within the given
388 displacement limits. This implies that such a system is less prone to catastrophic failure and, if failure were to occur,
389 it would be by progressive accumulation of displacements and serviceability failure.

390 Generally, when a non-stabilizing response is observed (commonly for the unreinforced case at $D/B=1.5, 2, 2.5$
391 under $CLR=40\%$ and uncommonly for the reinforced case at $D/B=1.5$ under $CLR=70\%$), due to excessive anchor
392 upward displacement, significant heave of the soil surface starts. This, in these unreinforced and reinforced cases,
393 local ruptures in the region above and around the anchor (punching failure), permit large displacements.

394

395 **3.6. Soil pressures over the anchor**

396 In order to demonstrate how soil pressure changes over the anchor during cyclic loading, in selected tests soil
397 pressure was measured through the two soil pressure cells (SPCi and SPCo). Fig. 17 shows the variation of measured
398 stress with time or loading cycle for an anchor with the embedment depth ratio of 2 ($D/B=2$) in both the unreinforced
399 and reinforced case. Fig. 17a-b illustrates the typical variation of change in soil pressures due to uplift loading, at a
400 point 100 mm above the anchor plate, 50 and 150 mm away from the center of anchor. As seen at the first, static,
401 phase of loading (approximately 0-25s), soil pressure within both pressure cells linearly increase to reach an
402 approximately constant value as the uplift load develops in the soil. It then remained constant (25-145s) until the
403 second phase of loading commenced (cyclic loading). In this cyclic load stage, the soil pressure near the center of
404 anchor (i.e. SPCi) increased with increasing cycle number. On the other hand, the soil pressure decreased at the
405 location of the outer pressure cell. Thus, with application of cyclic loading, load spreading becomes less effective with
406 stress becoming more concentrated in the zone where, for other installations, punching failure would occur. While

407 shear dislocation has not developed, it is clear that cyclic loading is beginning to redistribute the stresses in such a
 408 way that dislocation might, eventually, be achieved.

409 **Fig. 17c-d** compare the inner and outer soil pressure peaks of each loading cycles for an anchor with the
 410 embedment depth ratio of 2 ($D/B=2$) in the unreinforced and reinforced cases at different cyclic load ratios. In both
 411 cases the local increase of soil pressure on the top of anchor center increases as CLR increases (causing failure of the
 412 unreinforced case at CLR=40% and soil pressure of 115 kPa) while the soil pressure away from the anchor decreases
 413 (after a small increase in the first few cycles of loading of the reinforced soil). Soil pressure in all reinforced cases is
 414 less than in the unreinforced cases regardless of the fact that the cyclic load ratio in all cases is higher for the reinforced
 415 system. Evidently, the reinforced system can distribute load over a larger area and this helps to generate a more even
 416 and consistent distribution of uplift stress in the overlying soil. As the cyclic load ratio increases, the soil pressure
 417 measured by the outer soil pressure cell (SPCo) decreases more rapidly with number of cycles. Another observation
 418 is that, as CLR increases, the stress distributed outwards from the anchor centerline remains high when the installation
 419 is reinforced. Thus, reinforcement benefit is increased at high load ratios and at more cycles – eventually the
 420 installation is adjusting to the loading with more stress being transferred to the geocell layer.

421 To more clearly demonstrate the effect of geocell reinforcement on uplift pressure dispersion, the net soil pressures
 422 change due to cyclic uplift load measured by SPCi and SPCo at the peak of the first and last loading cyclic for $D/B=2$
 423 and different cyclic load ratios, are shown in **Table 4**. To evaluate the efficiency of reinforcement on distribution of
 424 uplift pressure over a larger area, two specific ratios, $\chi_{unrein.}$ and $\chi_{rein.}$ are introduced:

$$\chi_{unrein.} = \frac{(SPCo)_{unrein.}}{(SPCi)_{unrein.}} \quad (1)$$

$$\chi_{rein.} = \frac{(SPCo)_{rein.}}{(SPCi)_{rein.}} \quad (2)$$

425 in which $(SPCo)_{unrein.}$ and $(SPCi)_{rein.}$ are the pressures measured in the unreinforced systems by the outer and inner
 426 pressure cells, respectively (Eq. 1); while Eq. 2 takes the same approach for the reinforced conditions. In all cases, the
 427 values of soil pressure measured by outer pressure cell are less than those measured by the inner pressure cell. In this
 428 way, $\chi_{unrein.}$ and $\chi_{rein.}$ values less than unity (as given in **Table 4**) indirectly show that soil pressure decreases away
 429 from the center of the anchor, but in all cases more reduction occurs for unreinforced case. Initial values of $\chi_{unrein.}$ and
 430 $\chi_{rein.}$ (i.e 1st in **Table 4**) are approximately 0.4 and 0.6 for unreinforced and reinforced case, respectively. Thus, even

431 at first cycling loop, more even distribution is achieved by the reinforced installation. The change of the χ value on
432 cycling is more pronounced at lower load ratio values than at higher ones, although reinforcement makes the reduction
433 due to cycling less significant, i.e. stress concentration due to cyclic load adaptation is more readily avoided by
434 reinforced soil.

435

436 ***3.7. Post-cycling Monotonic Behavior of Unreinforced and Reinforced Anchor Systems***

437 After stable cyclic loading, monotonic loading was applied to the anchor until failure occurred, highlighting the
438 influence of cyclic loading on the degradation or increase of the ultimate capacity of anchor systems. **Fig. 18** shows
439 the load-displacement curve for initial monotonic loading, cyclic loading and post-cycling monotonic loading for
440 $D/B=2.0$ and CLR of 30% and 60% for unreinforced and reinforced beds, respectively. **Rao and Prasad (1991)** reported
441 a slight increase in post-cyclic loading capacity (i.e. the capacity of anchors subjected to the monotonic loading after
442 a period of cyclic loading) under low amplitude cyclic loading (CLR less than 20%) and a reduction in the post-cycling
443 uplift capacity with increase of CLR . Furthermore, the reinforced case shows more consistent post-peak ductile
444 response, undergoing considerable displacement without significant loss of strength. On the other hand, there is a large
445 reduction observing in the residual capacity (i.e. observation of increasing displacement with little change in loading
446 or achieving an upward displacement of 20 mm) for the unreinforced case.

447 For unreinforced conditions, post-cycling loading was only applied at two different load levels - CLR of 20% and
448 30%. For reinforced conditions, post-cycling loads were applied at CLR of 40%, 50%, 60% and 70%. **Fig. 19** compares
449 the post-cycling monotonic uplift loads following different cyclic load levels for both unreinforced and reinforced
450 conditions at D/B of 2. The general trend of uplift load versus upward displacement for post-cycling static load (**Fig.**
451 **19**) is same as for the purely static loading (c.f. **Fig. 5**), but there are some key differences. A distinct peak uplift load
452 was observed for unreinforced conditions whereas no distinct peak was observed for reinforced conditions as shown
453 in **Fig. 19**. This is also evident for the monotonic-only results (**Fig. 5**). The geocell-reinforced systems exhibited a
454 stiffer response than the unreinforced system (**Rahimi et al., 2018b**). Post-cycling monotonic loading, even at small
455 CLR , show a non-negligible reduction in both unreinforced peak and residual loads with the largest cyclic loads
456 resulting in the greatest reduction in subsequent monotonic load capacity.

457 **Table 5** shows a detailed summary of post-cycling monotonic loading at different embedment depths and cyclic load
458 levels. Less than a 5% reduction is observed in the uplift capacity of the reinforced bed at the failure load level of the
459 unreinforced case (CLR=40%), i.e. hardly any damage has been caused to the reinforced system under cyclic loading.
460 This advantage is more significant in comparison to the equivalent reduction for the unreinforced installation, which
461 is about 8% but at a much lower cyclic load level. At higher cyclic load levels there is a 15% reduction in both the
462 peak and residual loads for the reinforced bed with CLR=40-70% whereas a 20% reduction occurs for peak and a 20-
463 30% reduction for residual loads in the unreinforced bed at CLR=20 and 30%, respectively. This reduction in strength
464 may be attributed to the progression of plastic deformation in the overburden material, which in the case of dense
465 materials, may result in some level of softening. The presence of the reinforcement may reduce this accumulation of
466 plastic strain within the overlying material during cyclic loading while also providing mechanical resistance against
467 uplift when brought to failure, demonstrating less pronounced post-cyclic loss of anchor capacity in comparison to
468 unreinforced conditions. It should be noted that this behavior may not be applicable to loose, cohesionless materials. For
469 example, [Rao and Prasad \(1991\)](#) reported up to 4% increase in post-cycling uplift capacity for low amplitude cyclic
470 loading (SLR+CLR≤50%) in loose soils, likely owing to localized densification. On the other hand, they reported up
471 to 20% decrease in post-cycling uplift capacity for heavily cyclic loaded condition due to the onset of strain
472 localization and plastic deformation in the soil. That is, the same phenomenon that may densify loose soils may also
473 loosen dense soils, subsequently decreasing post-cycling anchor uplift capacity ([Schivan et al., 2017](#)). This
474 phenomenon illustrates the importance of considering both the peak and residual conditions when assessing ultimate
475 anchor capacity in design. Overall, the reinforced bed has two main advantages in comparison to the unreinforced
476 system (1) resistance against high cyclic loads and (2) post-cycling behavior without loss of peak and residual uplift
477 capacity, which are very useful for long-term application of anchor to the environments that are prone to frequent
478 cyclic loading.

479 **4. Summary and Conclusions**

480 This study presents the results of a set of experiments on the behavior of unreinforced and geocell-reinforced
481 anchor plates placed in sand and subject to both monotonic and cyclic uplift loading. The cyclic and monotonic post-
482 cycling responses of plate anchor buried in three different embedment depths in soil were evaluated. The experimental
483 tests were performed with a fixed sustained load (ratio being 30% of the monotonic ultimate static uplift capacity of

484 the unreinforced bed) followed by cyclic load testing at various amplitudes for ≤ 250 cycles. The findings described
485 below are valid for plate anchors of similar conditions of geometry, embedment depth, soil density, soil moisture, soil
486 grain sizes and cyclic loading parameters. Key conclusions are as follows:

- 487 • Two general types of load-displacement behavior were observed under cyclic loading – a stable or unstable
488 response. A stable response, characterized by decreasing rates of uplift displacement accumulation and by
489 hysteresis loops of reducing area, was observed in most reinforced tests and in unreinforced cases subject to
490 lower levels of loading. For unreinforced conditions, a *CLR* of 40% was identified as the threshold between
491 a stable and unstable response.
- 492 • Accumulated displacement increases with cyclic load ratio and decreases with embedment depth ratio. The
493 rate of accumulated displacement reaches a constant value after about 10 loading cycles. For the given
494 geometry and materials, sustained displacement rates of more than 0.05 mm/cycle were indicative of likely
495 progressive failure under excessive accumulated displacement.
- 496 • Where large cumulative displacements and unstable conditions occurred in unreinforced anchoring
497 configurations ($D/B=1.5, 2, 2.5$ under $CLR=40\%$) geocell reinforcement prevented excessive displacements.
498 The maximum anchor upward displacement is decreased relative to the unreinforced scenario for all cyclic
499 load ratios. The reinforced system exhibited a stable response under high amplitude cyclic loading. With the
500 exception of one test ($D/B=1.5$ under $CLR=70\%$), failure was not observed for reinforced conditions subject
501 to *CLR* of 40, 50, 60 and 70%.
- 502 • For the unstable response (unreinforced case at $D/B=1.5, 2, 2.5$ under $CLR=40\%$ and reinforced case at
503 $D/B=1.5$ under $CLR=70\%$), the excessive anchor upward displacement causes significant heave of the soil
504 surface local to the anchor rod.
- 505 • With an increasing number of loading cycles, the uplift pressure increases dramatically in the zone near to
506 the axis of anchor, and diminishes at the edge of anchor, particularly in the unreinforced case. Comparison
507 of soil pressure measured by inner and outer pressure cells (i.e. *SPCi* and *SPCo*) reveals that, under cyclic
508 loading, stresses tend to be concentrated around the soil near the anchor rod, while the presence of
509 reinforcement tends to distribute stresses over a larger area, preventing or delaying shear localization and
510 improving anchor stability.

- 511 • The post-cycling anchor load capacity of both the reinforced and unreinforced systems was less than their
512 respective original static load capacities. The greatest reduction from initial to final monotonic load capacities
513 was found in those installation that had received the largest magnitude of cyclic load amplitude. At the same
514 cyclic stress level, more damage was observed (by means of the reduction from initial to final monotonic –
515 peak and residual – load capacities) in the unreinforced than in the reinforced installations.

516 The experimental results were obtained for only one type of soil, one type of geocell characteristics and one
517 size of geocell (i.e. height and pocket). In spite of these limitations, the uplift tests provide insight into the possible
518 use of geocell reinforcement in anchoring applications. Added testing on other soils, reinforcement types and full-
519 scale conditions would further support its use in field application. Although the results provide an improved
520 understanding of cyclic uplift behavior considering geocell reinforcements, it is critical that alternative
521 configurations be scaled appropriately. This study, however, is insightful to represent near full-scale conditions
522 and could be helpful in designing large-scale anchor model tests and their simulation by numerical models and
523 methods. The presented results could possibly be generalized to different cyclic conditions, but this would require
524 careful consideration of scale, particularly relating to larger anchor plate sizes, different soil properties (density
525 and strength) and different geocell material properties. Although the general mechanisms and behavior observed
526 in the model tests could be reproduced in real applications, further tests with large-scale model anchor plates
527 should be conducted to validate the present findings at larger scales to determine the associated scale effects.
528 Dimensional analyses may provide scaling laws that enable conversion of design parameters from model tests to
529 more realistic dimensions used in design (e.g. scaling by a factor of λ , representative of the ratio of width of
530 prototype anchor plate to width of model anchor plate). By using the scaling law proposed by Langhaar (1951)
531 and dimensional analysis of Buckingham (1914), it was deduced that the reinforcement used at full-scale requires
532 a stiffness λ^2 times that of reinforcements used in the model tests to attain similar results, while the geometric
533 should be increased by λ . However, such conclusions should be validated in full-scale tests.

534 However, future work could extend the presented study to assess relevant design parameters, such as density
535 and mechanical properties of soil, plate size, embedment depth, anchor type, reinforcement geometric
536 configuration, and stiffness of geosynthetic materials. Future work could also consider the influence of geocell-
537 infill interaction properties such as roughness and shape, type and stiffness of geosynthetic materials and presence

538 of perforations to take into account the influence of varying geocell specification. In addition, different patterns
539 of cyclic loading and loading frequency can be considered in future studies.

540

541 *Acknowledgment*

542 The authors thank DuPont de Nemours, Luxembourg, and their UK agents, TDP Limited, for providing the
543 geocell reinforcement used in this test program.

544 *References*

- 545 ASTM. 2007. Standard test method for density and unit weight of soil in place by the sand-cone method. D1556-07.
546 ASTM International, West Conshohocken, PA.
- 547 ASTM. 2011. Standard practice for classification of soils for engineering purposes (unified soil classification
548 system). D2487-07. ASTM International, West Conshohocken, PA.
- 549 ASTM. 2012. Standard test methods for laboratory compaction characteristics of soil using modified effort. D1557-
550 12. ASTM International, West Conshohocken, PA.
- 551 Andreadis, A., and Harvey, R.C. 1979. An embedded anchor with an improved response to repeated loading. Applied
552 Ocean Research, **1**(4): 171-176.
- 553 Andreadis, A., and Harvey, R.C. 1981. A design procedure for embedded anchors. Applied Ocean Research, **3**(4):
554 177-182.
- 555 Basack, S., Indraratna, B., and Rujikiatkamjorn, C. 2015. Modeling the performance of stone column–reinforced soft
556 ground under static and cyclic loads. *Journal of Geotechnical and Geoenvironmental Engineering*, **142**(2): 1-
557 15.
- 558 Buckingham, E. 1914. On physically similar systems. *Physical Revision*, **4**: 345–376.
- 559 Byrne, B.W. 2000. Investigations of suction caissons in dense sand. Doctoral dissertation, University of Oxford.
- 560 Consoli N.C., Thomé A., Girardello V., and Ruver C.A., 2012. Uplift behavior of plates embedded in fiber-reinforced
561 cement stabilized backfill. *Geotextiles and Geomembranes*, **35**: 107–111
- 562 Choudhury, D., and Subba Rao, K. S., 2005. Seismic uplift capacity of inclined strip anchors. *Canadian Geotechnical*
563 *Journal*, **42**(1): 263-271.

- 564 Choudhary, A.K., and Dash, S.K., 2013. Uplift behaviour of horizontal plate anchors embedded in geocell-reinforced
565 sand, Proc. Indian Geotechnical Conference. Roorkee, India.
- 566 Dash, S.K., and Choudhary, A.K. 2018. Geocell reinforcement for performance improvement of vertical plate anchors
567 in sand. *Geotextiles and Geomembranes*, **46**(2): 214-225.
- 568 Datta, M., Gulhati, S.K., and Achari, G. 1990. Behavior of plate anchors in soft cohesive soils under cyclic loading.
569 *Indian Geotechnical Journal*, **20**(3): 206-224.
- 570 Fredlund, D. G. 2006. Unsaturated soil mechanics in engineering practice. *Journal of geotechnical and*
571 *geoenvironmental engineering*, **132**(3): 286-321.
- 572 Hegde, A. 2017. Geocell reinforced foundation beds-past findings, present trends and future prospects: A state-of-the-
573 art review. *Construction and Building Materials*, **154**: 658-674.
- 574 Herrmann, H. G. 1981. Design procedures for embedment anchors subjected to dynamic loading conditions (No.
575 NCEL-TR-888). Naval Civil Engineering Lab Port Hueneme, CA.
- 576 Indraratna, B., Biabani, M.M., and Nimbalkar, S. 2014. Behavior of geocell-reinforced subballast subjected to cyclic
577 loading in plane-strain condition. *Journal of Geotechnical and Geoenvironmental Engineering*, **141**(1): 1-16.
- 578 Kargar, M., and Mir Mohammad Hosseini, S. M. 2018. Influence of reinforcement stiffness and strength on load-
579 settlement response of geocell-reinforced sand bases. *European Journal of Environmental and Civil*
580 *Engineering*, **22**(5): 596-613.
- 581 Koerner, R.M. 1998. *Designing with geosynthetics*. Upper Saddle River, NJ: Prentice Hall.
- 582 Koshy, N., Unnikrishnan, N. 2016. Geosynthetics under cyclic pullout and post-cycling monotonic loading.
583 *International Journal of Geosynthetics and Ground Engineering*, **2**(2): 13.
- 584 Langhaar, J. L., 1951. *Dimensional Analysis and Theory of Models*, Wiley, New York, NY, USA.
- 585 Mengelt, M., Edil, T.B., and Benson, C.H. 2006. Resilient modulus and plastic deformation of soil confined in a
586 geocell. *Geosynthetics International*, **13**(5): 195-205.
- 587 Moghaddas Tafreshi, S.N., Dawson, A.R., 2010. Behaviour of footings on reinforced sand subjected to repeated
588 loading – Comparing use of 3D and planar geotextile. *Geotextiles and Geomembranes* **28**(5): 434–447.
- 589 Moghaddas Tafreshi, S. N., Javadi, S., Dawson, A.R., 2014a. Influence of geocell reinforcement on uplift response of
590 belled piles, *Acta Geotechnica*, **9**(3): 513–28.
- 591 Moghaddas Tafreshi, S.N., Khalaj, O., Dawson, A.R. 2014b. Repeated loading of soil containing granulated rubber

- 592 and multiple geocell layers. *Geotextiles and Geomembranes*, **42** (1): 25-38.
- 593 Ngo, N.T., Indranata, B., Rujikiatkamjorn, C., Biabani, M. 2015. Experimental and discrete element modeling of
594 geocell-stabilized subballast subjected to cyclic loading. *Journal of Geotechnical and Geoenvironmental*
595 *Engineering*, **142**(4): 1-16.
- 596 Pérez, Z., Schiavon, J.A., Tsuha, C.H.C., Dias, D., and Thorel, L. 2018. Numerical and experimental study on the
597 influence of installation effects on the behaviour of helical anchors in very dense sand. *Canadian*
598 *Geotechnical Journal*, **55**(8): 1067-1080.
- 599 Petereit, R.A. 1987. The static and cyclic pullout behavior of plate anchors in fine saturated sand. Doctoral dissertation,
600 Oregon State University, Corvallis.
- 601 Ponniah, D.A., and Finlay, T.W. 1988. Cyclic behaviour of plate anchors. *Canadian Geotechnical Journal*, **25**(2): 374-
602 381.
- 603 Prasad, Y.V.S.N., and Rao, S.N. 1994. Experimental studies on foundations of compliant structures—II. Under cyclic
604 loading. *Ocean engineering*, **21**(1): 15-27.
- 605 Rao, S.N., and Prasad, Y.V.S.N. 1991. Behavior of a helical anchor under vertical repetitive loading. *Marine*
606 *Georesources and Geotechnology*, **10**(3-4): 203-228.
- 607 Rahimi, M., Leshchinsky, B. and Moghaddas Tafreshi, S.N. 2018a. Assessing the ultimate uplift capacity of plate
608 anchors in geocell-reinforced sand. *Geosynthetics International*, **00**, No. **0**, 1–18.
609 [<https://doi.org/10.1680/jgein.18.00029>]
- 610 Rahimi, M., Moghaddas Tafreshi, S.N., Leshchinsky, B., and Dawson, A.R. 2018b. Experimental and numerical
611 investigation of the uplift capacity of plate anchors in geocell-reinforced sand, *Geotextiles and*
612 *Geomembranes*, **46** (6): 801-816.
- 613 Ravichandran, P.T., Ilamparuthi, K., and Toufeeq, M.M. 2008. Study on uplift behaviour of plate anchors under
614 monotonic and cyclic loading in geo-grid reinforced sand bed. The 12th International Conference of
615 International Association for Computer Methods and Advances in Geomechanics (IACMAG), Goa, India.
616 3448-3455.
- 617 Satyal, S., Leshchinsky, B., Han, J. and Neupane., M. 2018. Use of cellular confinement for improved railway
618 performance on soft subgrades: a numerical study. *Geotextiles and Geomembranes*, **46**(2): 190-205.

- 619 Schiavon, J.A. 2016. Behaviour of helical anchors subjected to cyclic loadings. Doctoral dissertation, Universidade
620 de São Paulo.
- 621 Schiavon, J.A., Tsuha, C.D.H.C., and Thorel, L. 2017. Cyclic and post-cycling monotonic response of a single-helix
622 anchor in sand. *Géotechnique Letters*, **7**(1): 11-17.
- 623 Singh, S.P., and Ramaswamy, S.V. 2008. Influence of frequency on the behaviour of plate anchors subjected to cyclic
624 loading. *Marine Georesources and Geotechnology*, **26**(1): 36-50.
- 625 Singh, S.P., and Ramaswamy, S.V. 2010. Effects of cyclic frequency and pre-loading on behaviour of plate anchors.
626 In *Deep Foundations and Geotechnical in Situ Testing*. 252-260.
- 627 Sitharam, T. G., and Hegde, A. 2013. Design and construction of geocell foundation to support the embankment on
628 settled red mud. *Geotextiles and Geomembranes*, **41**: 55-63.
- 629 Stuyts, B., Cathie, D., Powell, T. 2016. Model uncertainty in uplift resistance calculations for sandy backfills.
630 *Canadian Geotechnical Journal*, **53**(11): 1831-1840.
- 631 Suku, L., Prabhu, S.S., Ramesh, P., and Babu, G.S. 2016. Behavior of geocell-reinforced granular base under repeated
632 loading. *Transportation Geotechnics*, **9**: 17-30.
- 633 Thakur, J.K., Han, J., and Parsons, R.L. 2016. Factors influencing deformations of geocell-reinforced recycled asphalt
634 pavement bases under cyclic loading. *Journal of Materials in Civil Engineering*, **29**(3): 1-8.
- 635 Thakur, J.K., Han, J., Pokharel, S.K., Parsons, R.L. 2012. Performance of geocell-reinforced recycled asphalt
636 pavement (RAP) bases over weak subgrade under cyclic plate loading. *Geotextiles and Geomembranes* **35**:
637 14-24.
- 638 Wang, D., and O'Loughlin, C.D., 2014. Numerical study of pull-out capacities of dynamically embedded plate
639 anchors. *Canadian Geotechnical Journal*, **51**(11): 1263-1272.
- 640 Wang, J.Q., Zhang, L.L., Xue, J.F., Tang, Y. 2018. Load-settlement response of shallow square footings on geogrid-
641 reinforced sand under cyclic loading. *Geotextiles and Geomembranes*, **46**(5): 586-596.
- 642 Werkmeister, S., Dawson, A., and Wellner, F. 2001. Permanent deformation behavior of granular materials and the
643 shakedown concept. *Transportation Research Record: Journal of the Transportation Research Board*, **1757**:
644 75-81.
- 645 Yu, L., Zhou, Q., and Liu, J. 2015. Experimental study on the stability of plate anchors in clay under cyclic loading.
646 *Theoretical and Applied Mechanics Letters*, **5**(2): 93-96.

647 Zhang, L., Zhao, M., Shi, C., and Zhao, H. 2010. Bearing capacity of geocell reinforcement in embankment
648 engineering. *Geotextiles and Geomembranes*, **28**(5): 475-482.

649

650

Nomenclature	
B	width of anchor plate
b	width of geocell mattress
CLR	cyclic load ratio ($CLR=P_c/P_u$)
CLR_{cr}	critical cyclic load ratio
d	geocell pocket size
D	embedment depth of anchor plate
G_s	specific gravity
h	height of geocell
P_c	ratio of cyclic load amplitude to monotonic ultimate uplift capacity of unreinforced installation
P_r	ultimate uplift capacity of reinforced installation
P_s	ratio of applied initial sustained load to monotonic ultimate uplift capacity of unreinforced installation
P_u	ultimate uplift capacity of unreinforced installation
SLR	sustained load ratio ($CLR=P_s/P_u$)
$SPCi$	inner soil pressure cell
$SPCo$	outer soil pressure cell
u_d	anchor upward displacement
γ	soil unit weight
λ	the ratio of width of prototype anchor plate to width of model anchor plate
ϕ	soil angle of internal friction
χ_{rein}	ratio of outer pressure cell (SPCo) to the inner pressure cell (SPCi) at reinforced condition
$\chi_{unrein.}$	ratio of outer pressure cell (SPCo) to the inner pressure cell (SPCi) at unreinforced condition

651

652

653 **List of Tables**

Table 1	Engineering properties of the geotextile used in the tests
Table 2	Densities of soil for unreinforced and geocell-reinforced layers after compaction
Table 3	Scheme of the uplift tests on anchor in unreinforced and geocell-reinforced backfills ($h=100$ mm, $b/B=3$, $SLR=30\%$)
Table 4	Comparison of measured soil pressure in unreinforced and geocell-reinforced systems corresponding to peak of first (1 st) and last (250 th) lading cycles
Table 5	Static post cyclic capacity comparison with ultimate static capacity

654

655

656

657

658 **List of Figures**

Fig. 1	Grain size distribution curves for backfill soil
Fig. 2	A view of geocell spread over the anchor plate in the test pit
Fig. 3	Test installation prior to loading (a) actual physical model and (b) Schematic representation (units in mm)
Fig. 4	Schematic diagram of loading pattern
Fig. 5	Load-displacement behavior of anchor plate (a) unreinforced case (b) reinforced case
Fig. 6	Typical trend response (a) stable anchor upward movement with time (b) stable load-displacement hysteresis (c) unstable anchor upward movement with time (d) unstable load-displacement hysteresis
Fig. 7	Variation of the anchor uplift displacements with cyclic loading for the unreinforced case under different cyclic load ratio for (a) $D/B=1.5$ (b) $D/B=2.0$ and (c) $D/B=2.5$
Fig. 8	Variation of the rate of upward displacement per cycle for the unreinforced case under different cyclic load ratio for (a) $D/B=1.5$ (b) $D/B=2.0$ and (c) $D/B=2.5$
Fig. 9	Anchor response at $CLR_{cr}=40\%$ and $D/B=2.0$ for unreinforced and reinforced case (a) upward displacement variation (b) load hysteresis
Fig. 10	Anchor response at $CLR_{cr}=40\%$ for reinforced and unreinforced (repeated) at different embedment depth ratios (a) variation of anchor movement (b) accumulated displacement rate
Fig. 11	Heave of soil surface at the end of the cyclic loading for $CLR=40\%$ and $D/B=2$ (a) unreinforced bed (b) reinforced bed
Fig. 12	Heave height at soil surface respect to anchor centerline at the end of the cyclic loading with $CLR=40\%$ (a) unreinforced bed (20 mm anchor displacement) (b) reinforced bed (after 250 loading cycles)
Fig. 13	Load displacement hysteresis for reinforced case at $D/B=2$ for different cyclic load ratios (a) $CLR=50\%$, (b) $CLR=60\%$ and (c) $CLR=70\%$
Fig. 14	Load displacement loop at 1st, 10th, 100th and 200th cycle for reinforced case at $D/B=2$ for different cyclic load ratios (a) $CLR=50\%$, (b) $CLR=60\%$ and (c) $CLR=70\%$
Fig. 15	Variation of the anchor upward movement with number of load cycles for the reinforced case under different cyclic load ratio for (a) $D/B=1.5$ (b) $D/B=2.0$ and (c) $D/B=2.5$
Fig. 16	Variation of the rate of upward displacement per cycle for the reinforced case under different cyclic load ratio for (a) $D/B=1.5$ (b) $D/B=2.0$ and (c) $D/B=2.5$
Fig. 17	Typical trend of soil pressure (a) at location of SPC_i (b) at location of SPC_o , soil pressure measured at $D/B=2$ and different CLR (c) unreinforced bed (d) reinforced bed
Fig. 18	Variation of the uplift load with anchor movement (a) unreinforced case, $D/B=2.0$ and $CLR=30\%$ (b) reinforced, $D/B=2.0$ and $CLR=60\%$

Fig. 19	Post-cycling behavior of anchor plate at $D/B=2$ and different cyclic load ratio, CLR (a) unreinforced case (b) reinforced case
---------	---

659

Draft

Table 1. Engineering properties of the geotextile used in the tests

Description	Value
Type of geotextile	Nonwoven
Material	Polypropylene
Area weight (gr/m ²)	190
Thickness under 2 kN/m ² (mm)	0.57
Thickness under 200 kN/m ² (mm)	0.47
Tensile strength (kN/m)	13.1
Strength at 5% (kN/m)	5.7
Effective opening size (mm)	0.08

Table 2. Densities of soil for unreinforced and geocell-reinforced layers after compaction

Type of layer	Average dry density (kN/m ³)
Unreinforced soil layer	≈18.78*
Geocell-reinforced layer	Between 18.2 and 18.4

*approximately 92% of maximum dry density – see Sec. 2.1.

Table 3. Scheme of the uplift tests on anchor in unreinforced and geocell-reinforced backfills (h=100 mm, b/B=3, SLR=30%)

Test Series	Type of Test	Cyclic Load Ratio, CLR (%)	Embedment Depth Ratio, D/B	No. of Tests	Purpose of the Tests
1	Monotonic unreinforced	-	1.5, 2, 2.5	3	Obtain the ultimate unreinforced capacity, performed first and comparison with post-cycling capacity.
2	Monotonic geocell-reinforced	-		3	Quantify additional capacity from reinforcement and comparison with post-cycling capacity.
3	Cyclic unreinforced	20, 30, 40		9	Understand cyclic behavior of loaded anchor systems.
4	Cyclic geocell-reinforced	40, 50, 60, 70		12	Quantify improvement of anchoring under cyclic loading.

Table 4. Comparison of measured net soil pressure change due to cyclic uplift load in unreinforced and geocell-reinforced systems corresponding to peak of first (1st) and last (250th) lading cycles

		Peak soil pressure corresponding to 1 st and 250 th loading cycles (kPa)											
D/B	CLR (%)	Unreinforced						Reinforced					
		SPCi		SPCo		$\chi_{unrein.}$		SPCi		SPCo		$\chi_{rein.}$	
		1 st	250 th	1 st	250 th	1 st	250 th	1 st	250 th	1 st	250 th	1 st	250 th
2	20	64	101	26	8	0.41	0.08	---	---	---	---	---	---
	30	76	113	31	8	0.41	0.08	---	---	---	---	---	---
	40	82	115*	35	31*	0.43	0.27	47	83	27	14	0.57	0.17
	50	---	---	---	---	---	---	53	86	31	16	0.58	0.19
	60	---	---	---	---	---	---	58	91	33	28	0.57	0.31
	70	---	---	---	---	---	---	62	102	36	40	0.58	0.40

* corresponding to pre-failure condition

Table 5: Static post cyclic capacity comparison with ultimate static capacity

CLR (%)	$P_{post-cycling}/P_{static}$ (%)											
	D/B=1.5				D/B=2.0				D/B=2.5			
	Peak		Res.		Peak		Res.		Peak		Res.	
	Unrein.	Rein.	Unrein.	Rein.	Unrein.	Rein.	Unrein.	Rein.	Unrein.	Rein.	Unrein.	Rein.
20	91	*	77	*	93	*	80	*	92	*	81	*
30	82	*	69	*	83	*	71	*	84	*	71	*
40	Fail	95	Fail	97	Fail	96	Fail	98	Fail	96	Fail	96
50	*	89	*	92	*	92	*	93	*	92	*	88
60	*	85	*	85	*	90	*	85	*	89	*	87
70	*	Fail	*	Fail	*	87	*	84	*	86	*	85

*Test was not performed in these cases

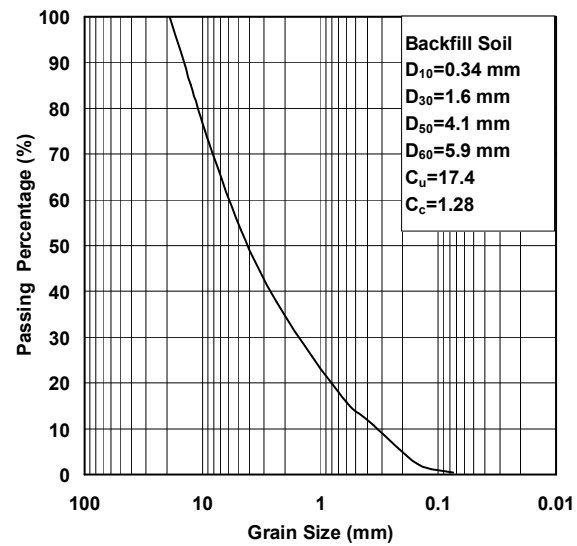


Fig. 1. Grain size distribution curves for backfill soil



Fig. 2. A view of geocell spread over the anchor plate in the test pit

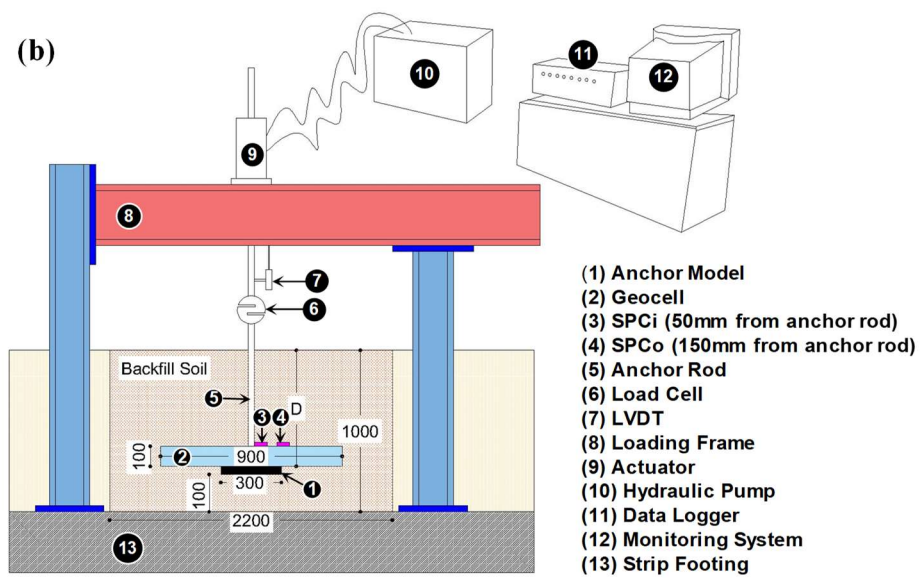
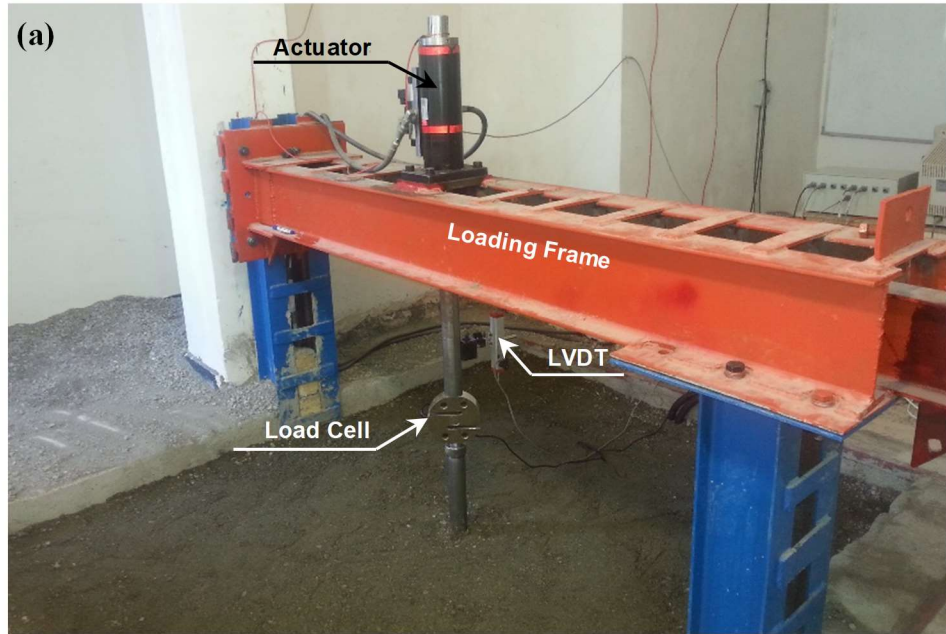


Fig. 3. Test installation prior to loading (a) actual physical model and (b) Schematic representation (units in mm)

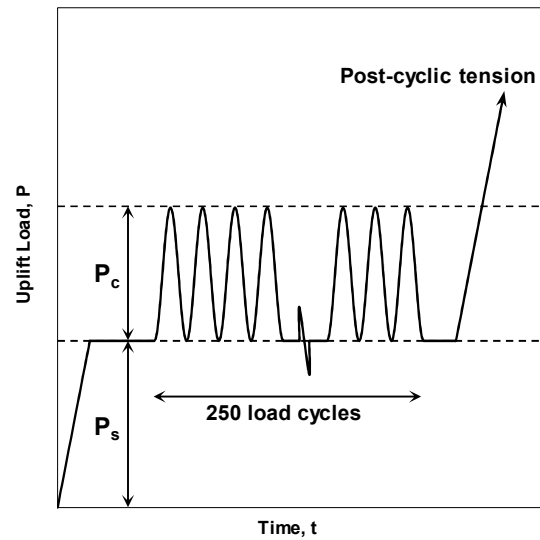


Fig. 4. Schematic diagram of loading pattern

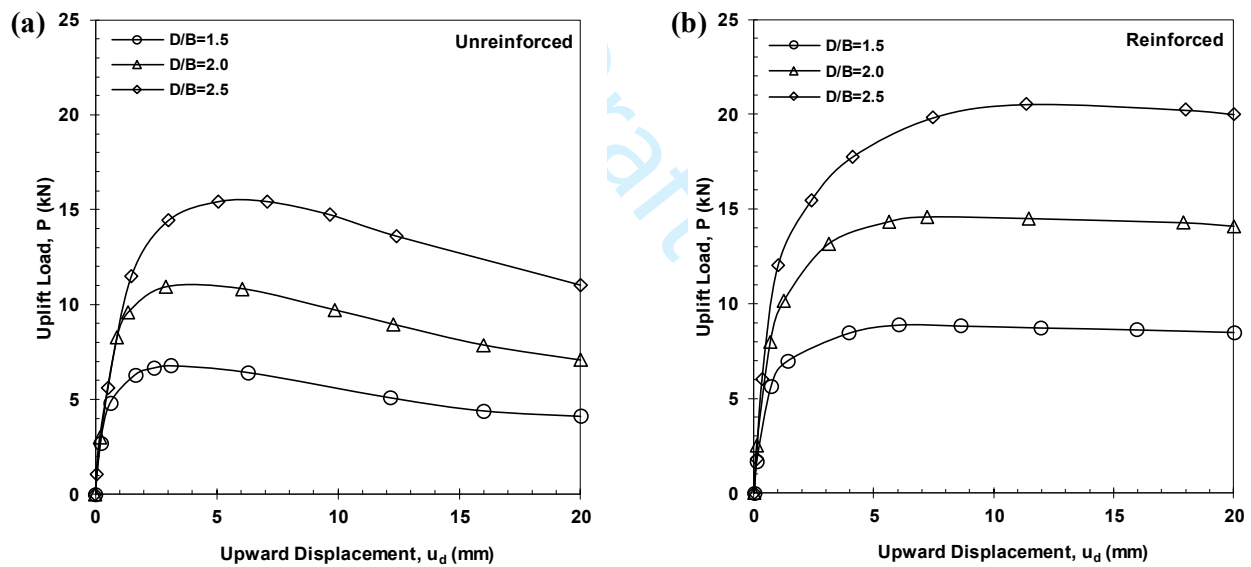


Fig. 5. Load-displacement behavior of anchor plate (a) unreinforced case (b) reinforced case

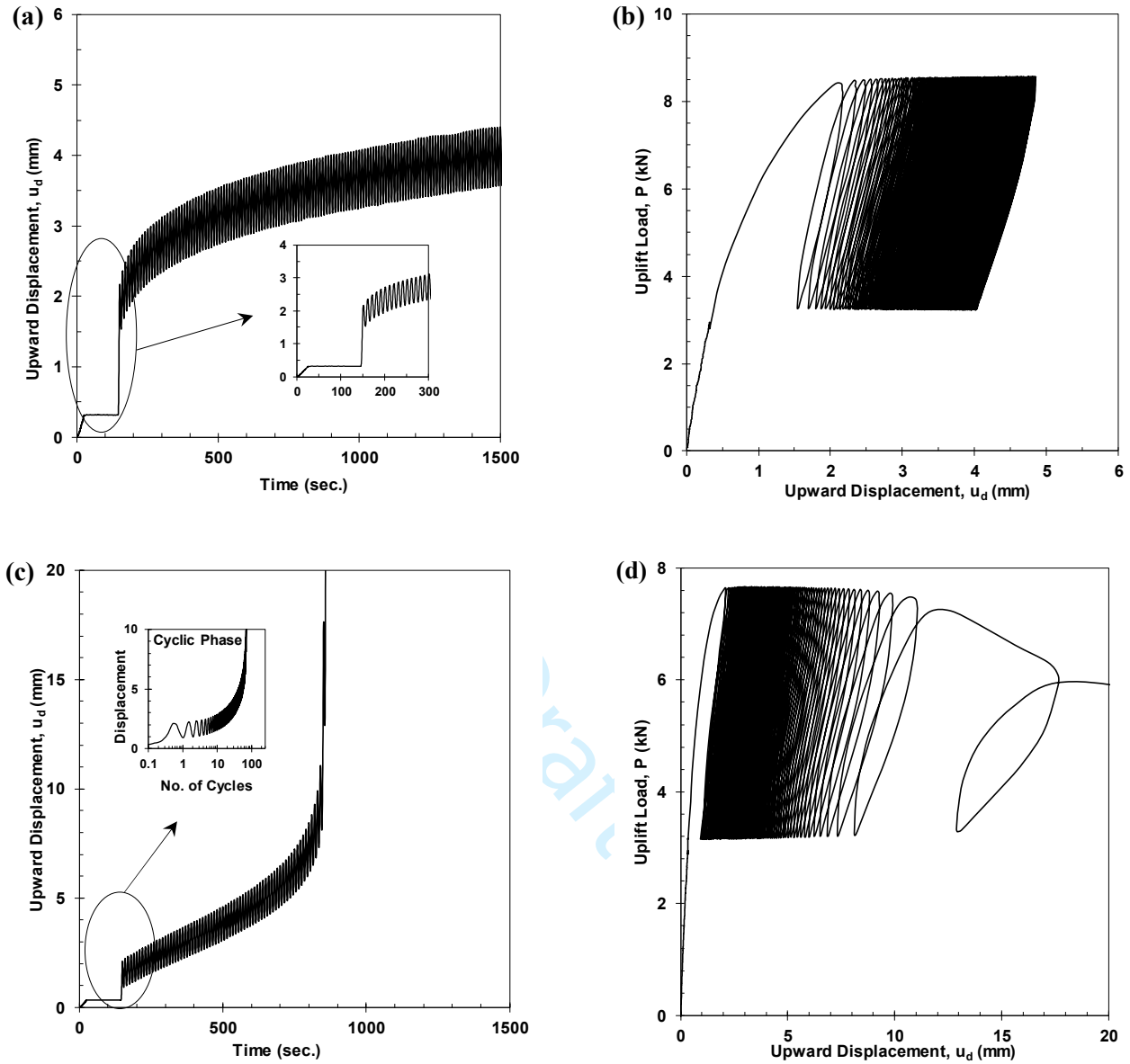


Fig. 6. Typical trend response (a) stable anchor upward movement with time (b) stable load-displacement hysteresis (c) unstable anchor upward movement with time (d) unstable load-displacement hysteresis

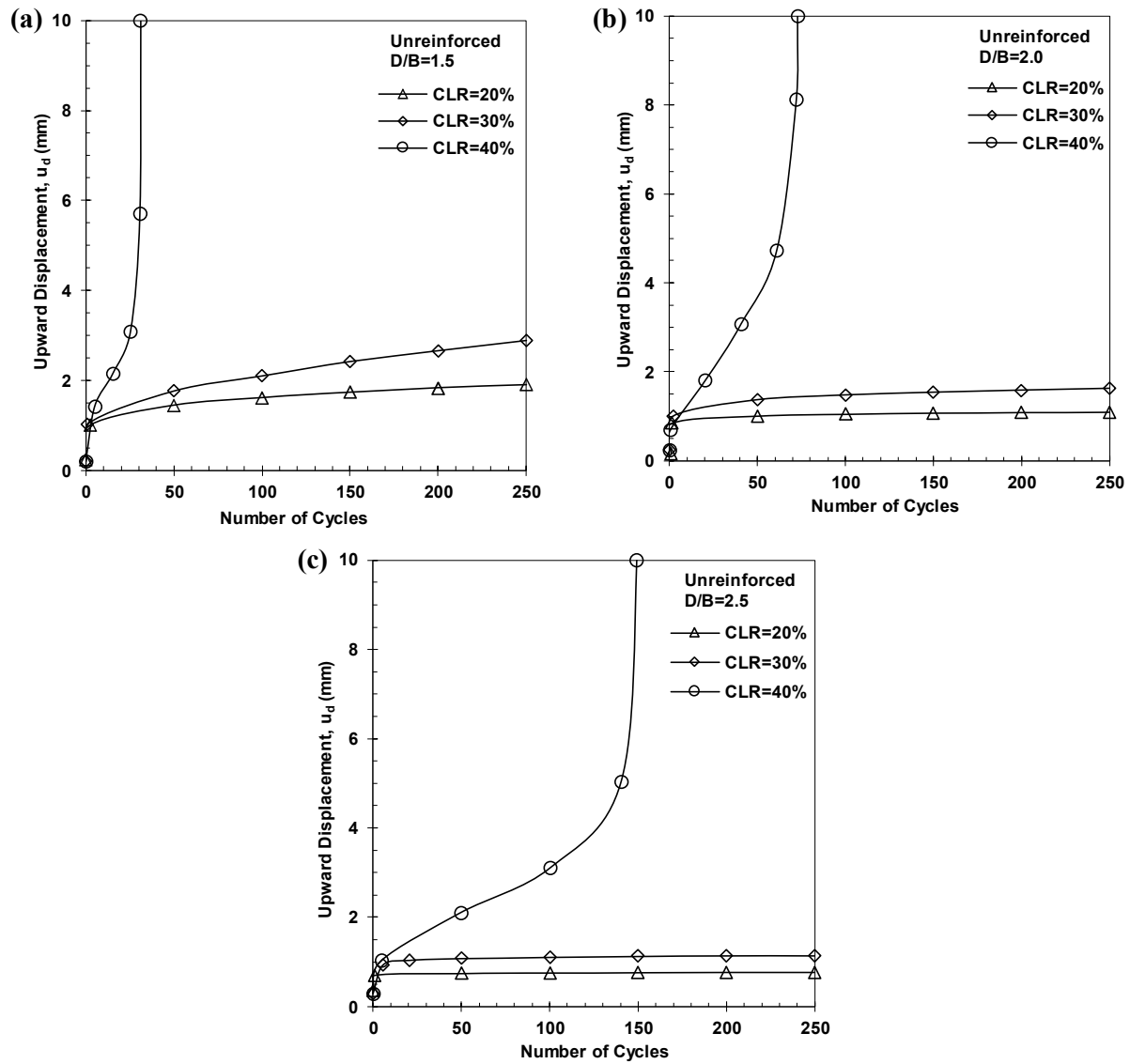


Fig. 7. Variation of the anchor uplift displacements with cyclic loading for the unreinforced case under different cyclic load ratio for (a) $D/B=1.5$ (b) $D/B=2.0$ and (c) $D/B=2.5$

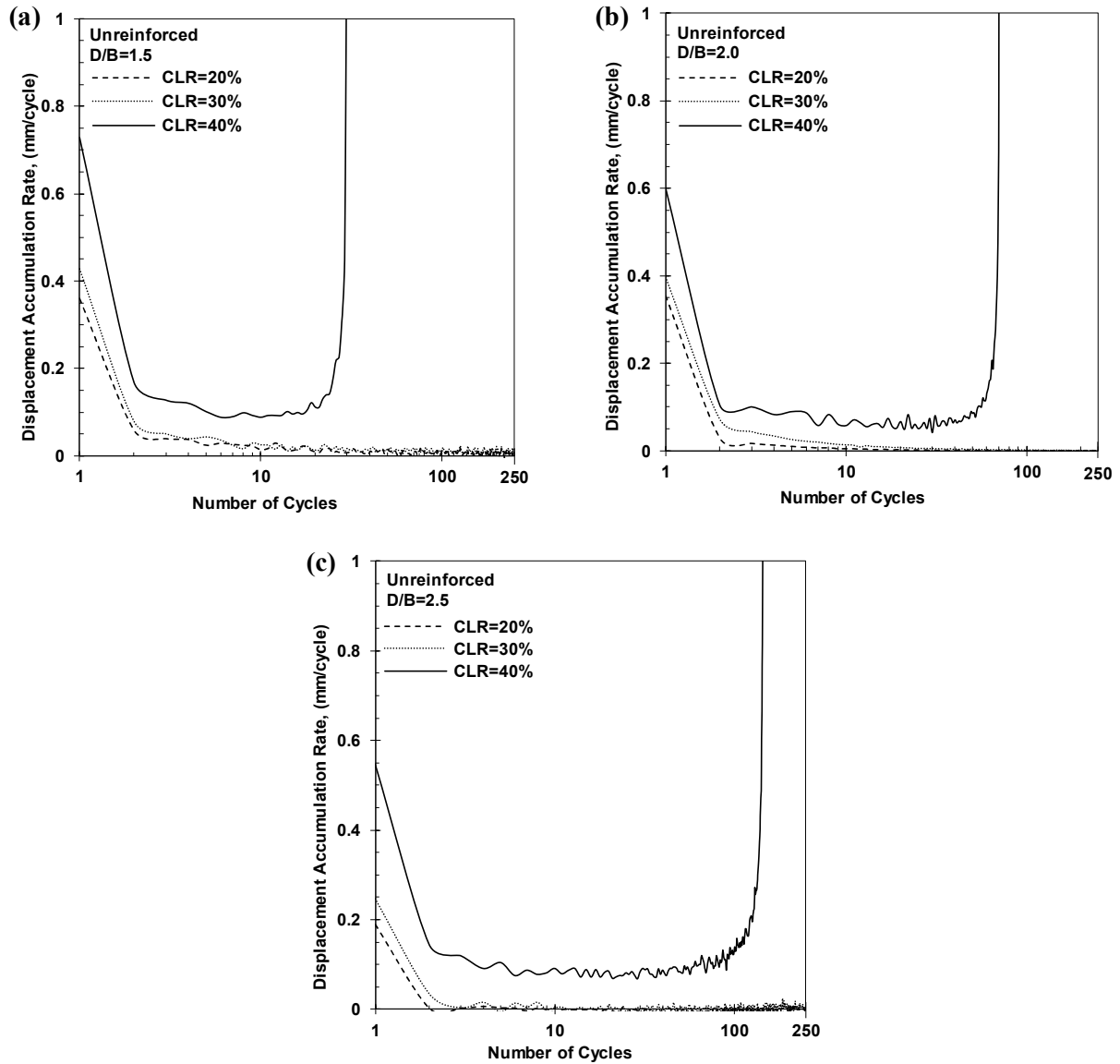


Fig. 8. Variation of the rate of upward displacement per cycle for the unreinforced case under different cyclic load ratio for (a) $D/B=1.5$ (b) $D/B=2.0$ and (c) $D/B=2.5$

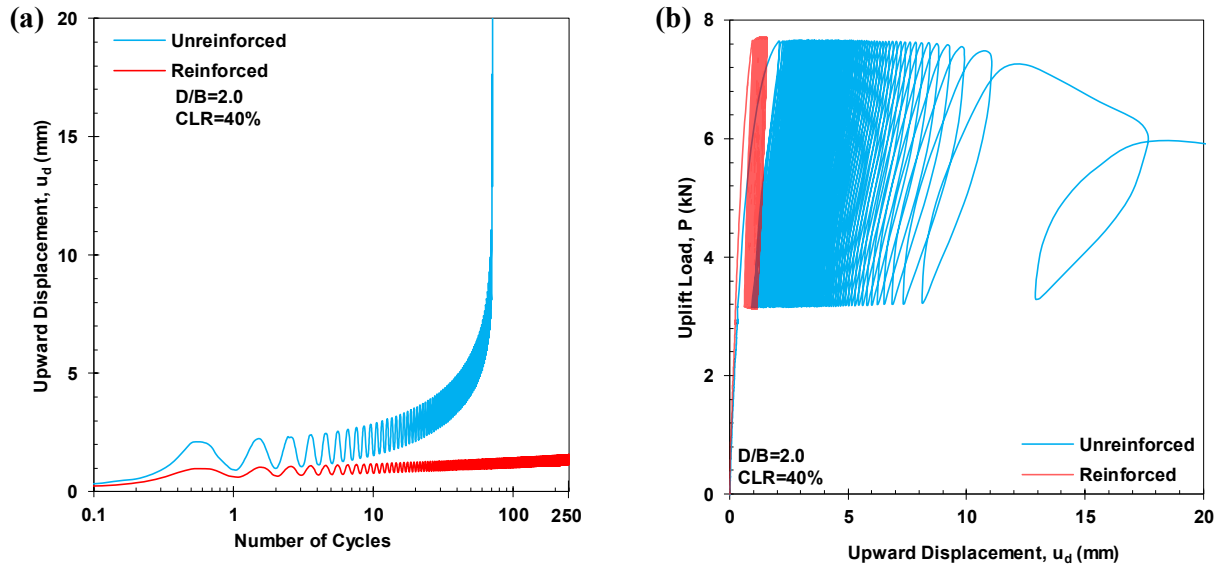


Fig. 9. Anchor response at $CLR_{cr}=40\%$ and $D/B=2.0$ for unreinforced and reinforced case (a) upward displacement variation (b) load hysteresis.

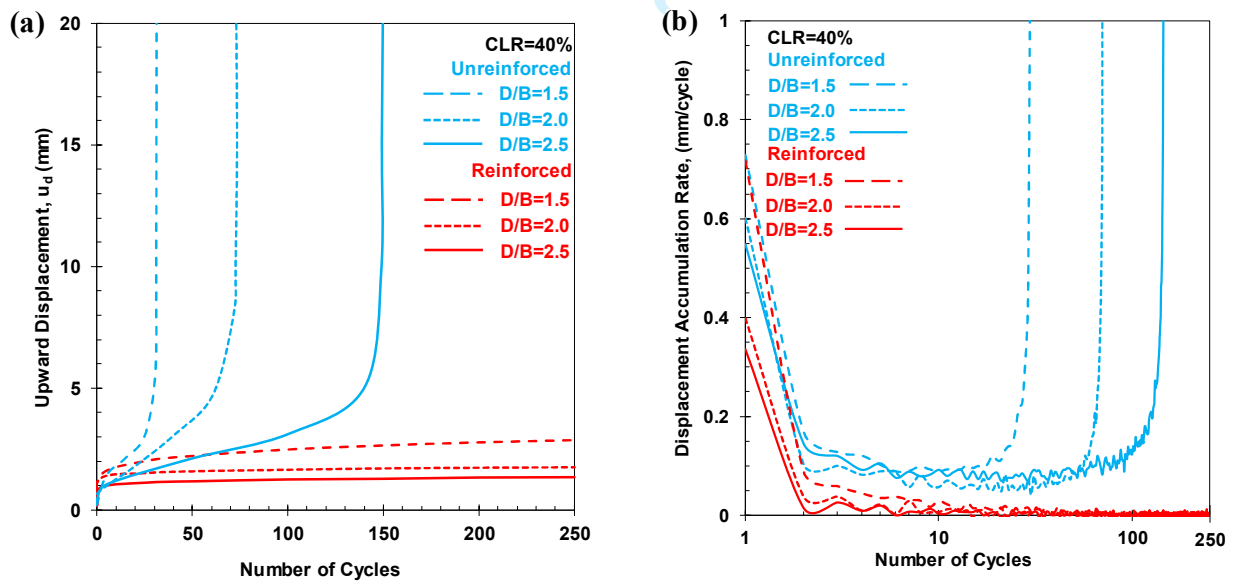


Fig. 10. Anchor response at $CLR_{cr}=40\%$ for reinforced and unreinforced (repeated) at different embedment depth ratios (a) variation of anchor movement (b) accumulated displacement rate

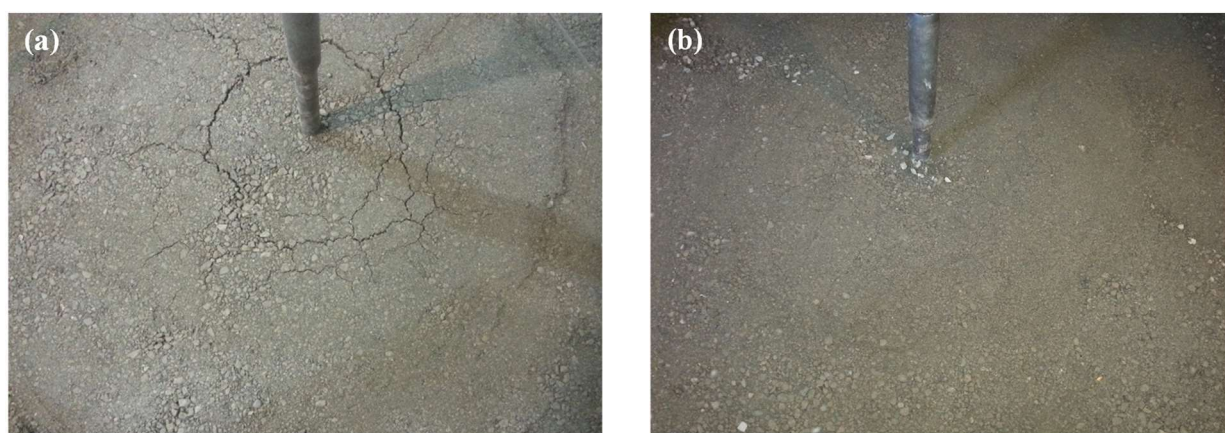


Fig. 11. Heave of soil surface at the end of the cyclic loading for $CLR=40\%$ and $D/B=2$ (a) unreinforced bed (b) reinforced bed

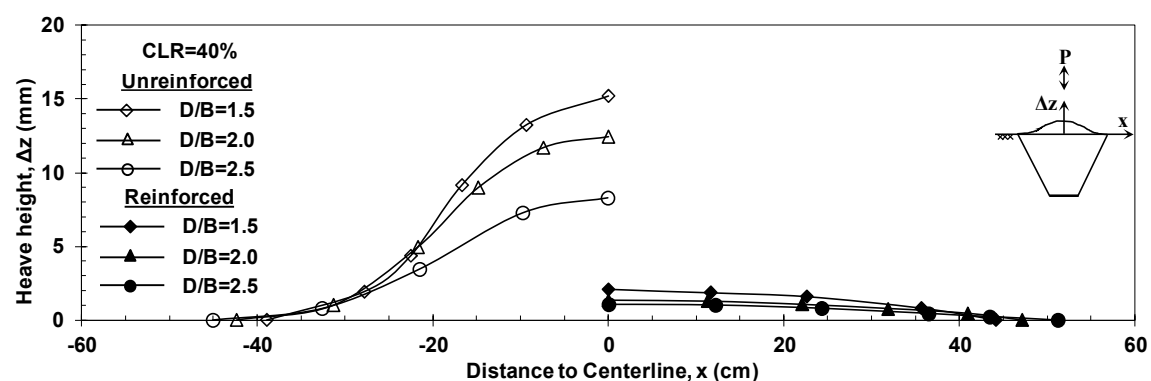


Fig. 12. Heave height at soil surface respect to anchor centerline at the end of the cyclic loading with $CLR=40\%$ for unreinforced bed (20 mm anchor displacement) and reinforced bed (after 250 loading cycles)

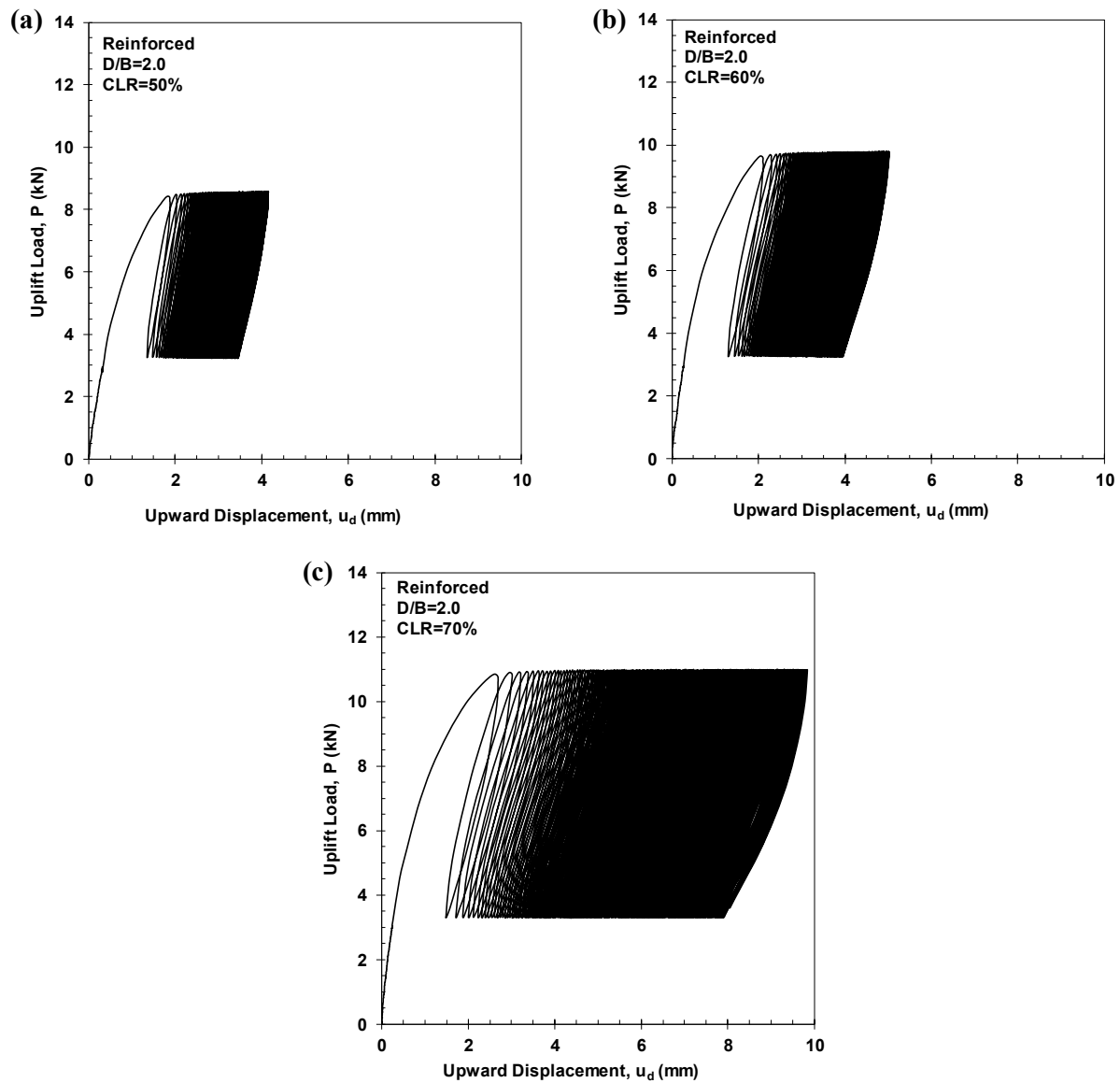


Fig. 13. Load displacement hysteresis for reinforced case at $D/B=2$ for different cyclic load ratios (a) $CLR=50\%$, (b) $CLR=60\%$ and (c) $CLR=70\%$

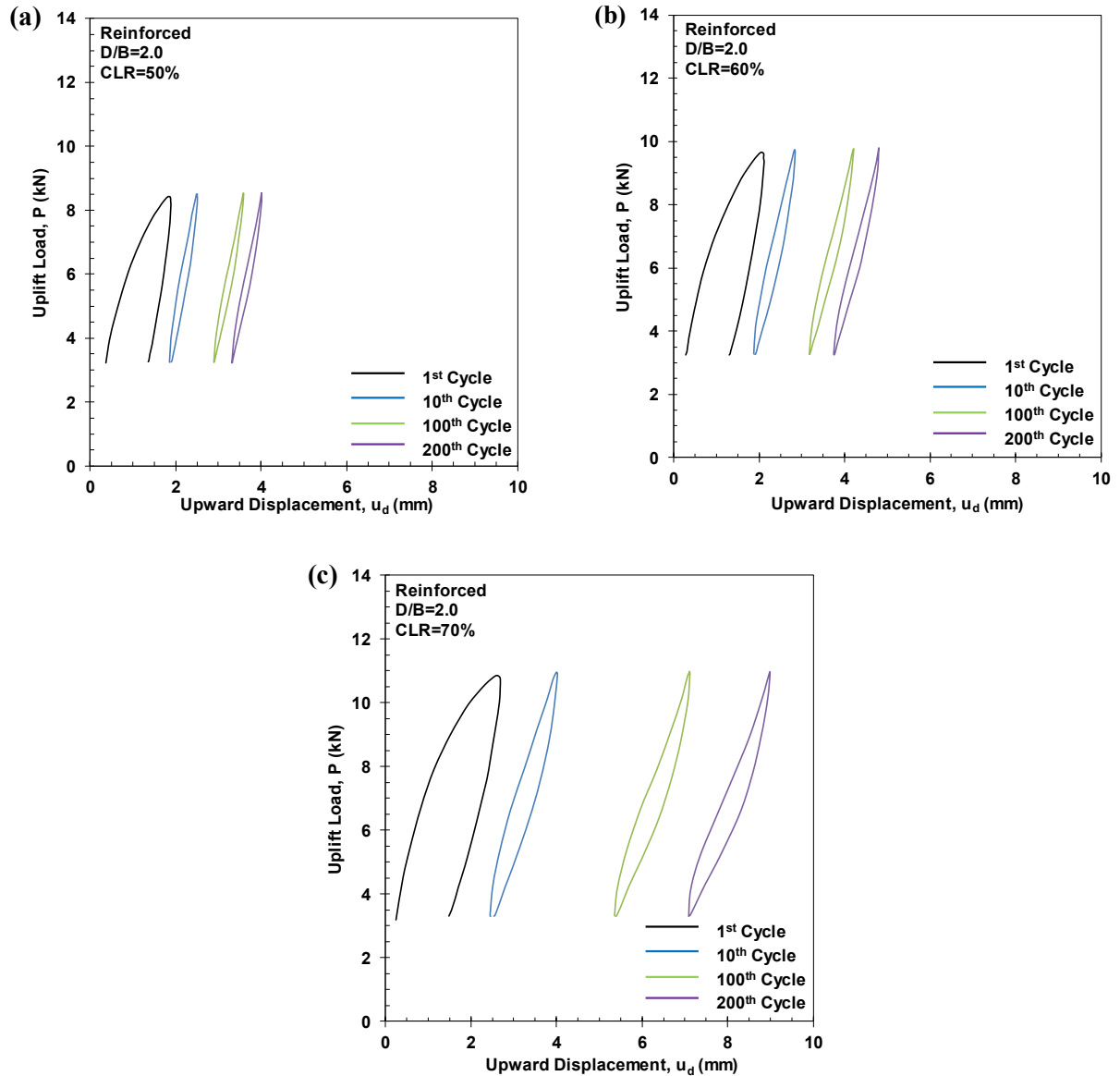


Fig. 14. Load displacement loop at 1st, 10th, 100th and 200th cycle for reinforced case at $D/B=2$ for different cyclic load ratios (a) CLR=50%, (b) CLR=60% and (c) CLR=70%

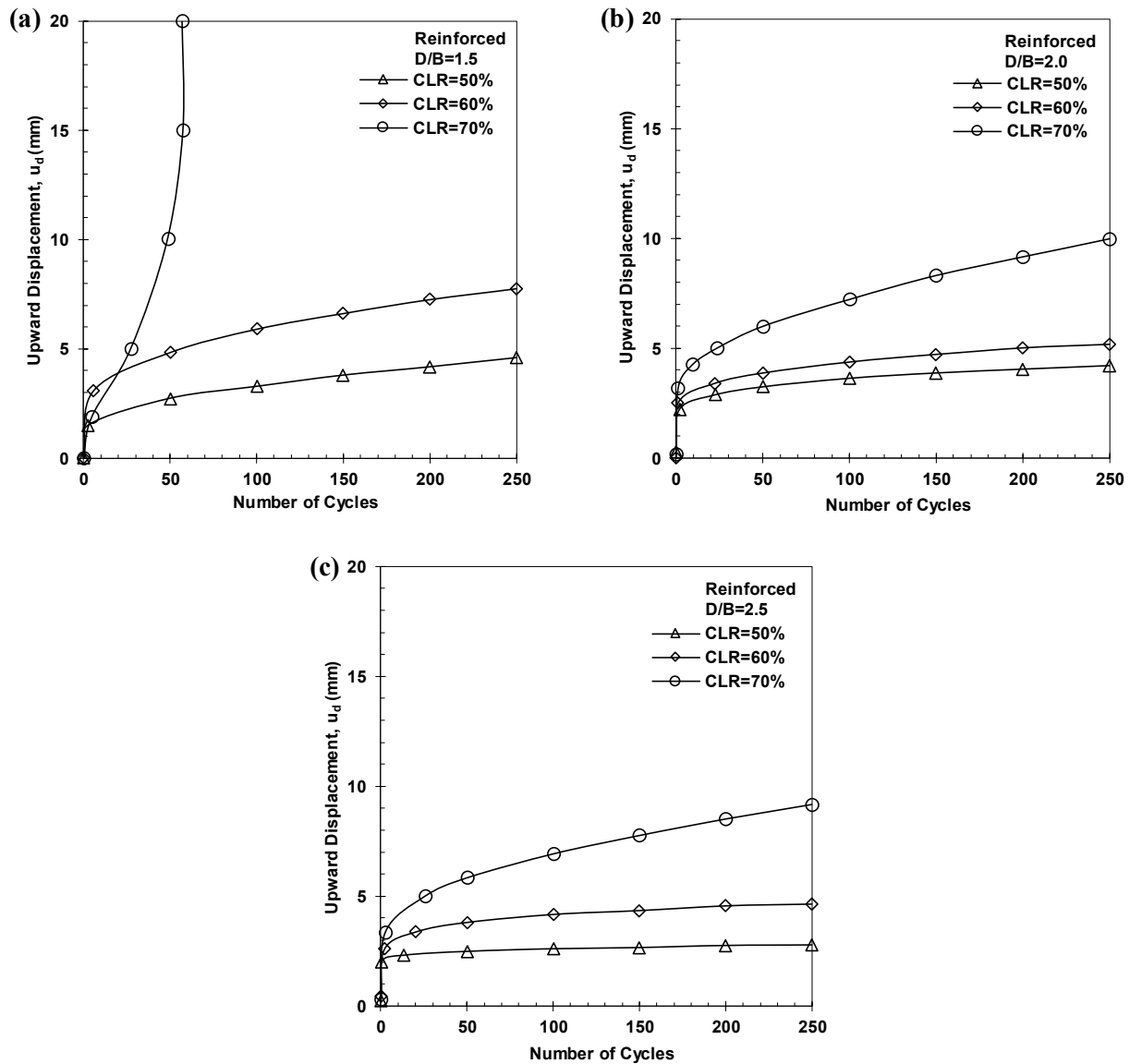


Fig. 15. Variation of the anchor upward movement with number of load cycles for the reinforced case under different cyclic load ratio for (a) $D/B=1.5$ (b) $D/B=2.0$ and (c) $D/B=2.5$

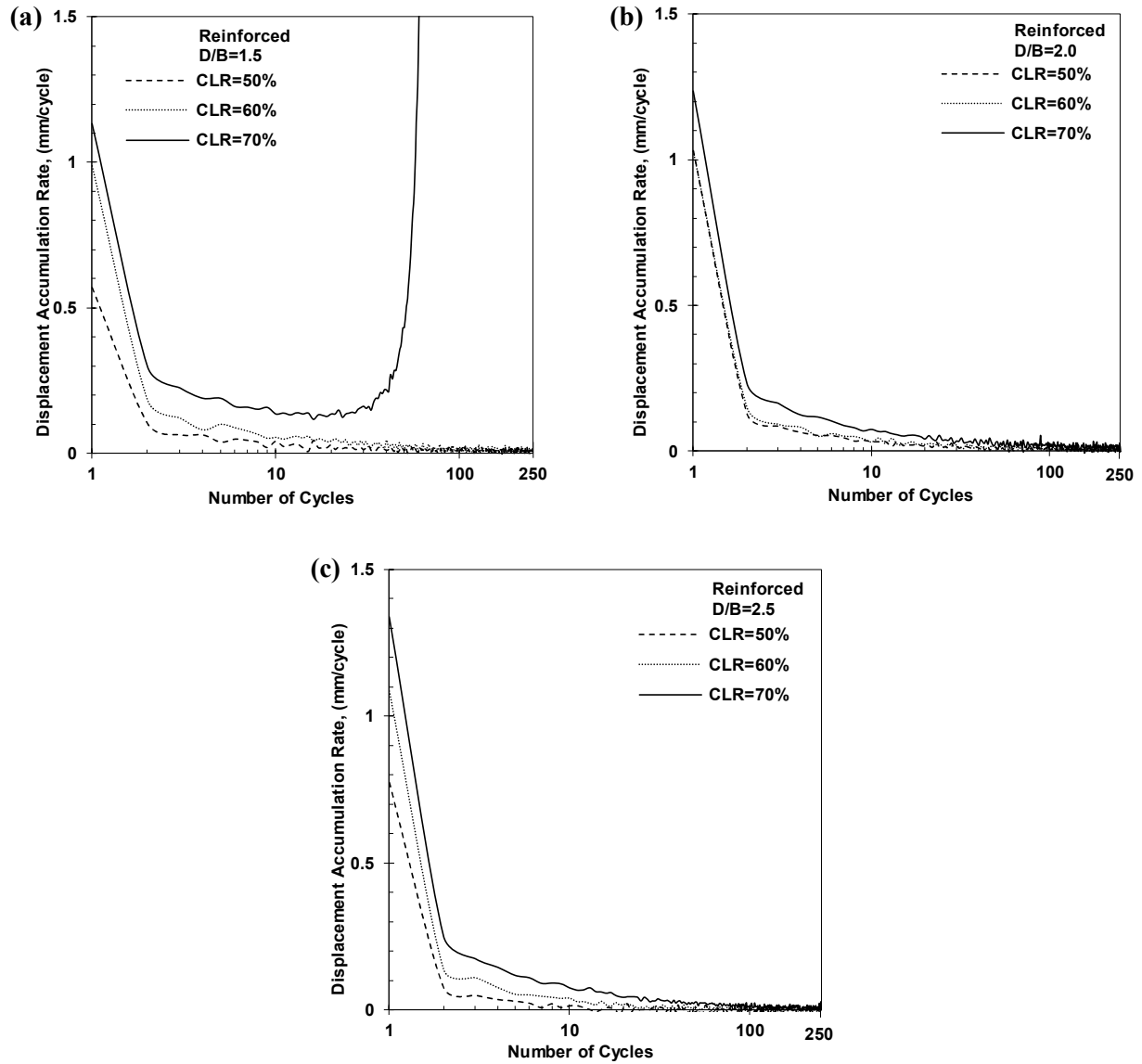


Fig. 16. Variation of the rate of upward displacement per cycle for the reinforced case under different cyclic load ratio for (a) $D/B=1.5$ (b) $D/B=2.0$ and (c) $D/B=2.5$

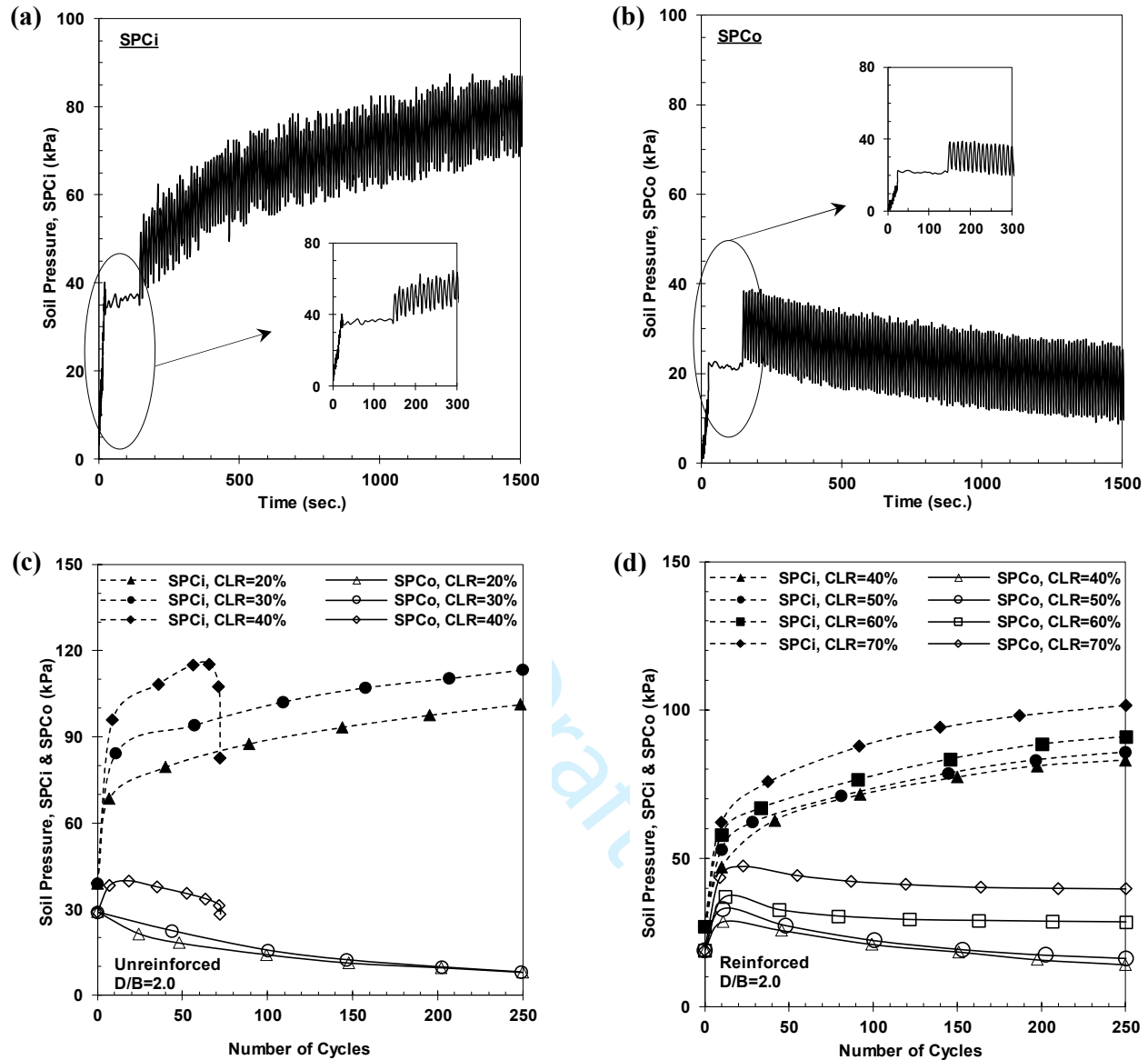


Fig. 17. Typical trend of soil pressure at location of (a) SPCi (b) SPCo, and soil pressure measured at $D/B=2$ under different CLR for (c) unreinforced bed (d) reinforced bed

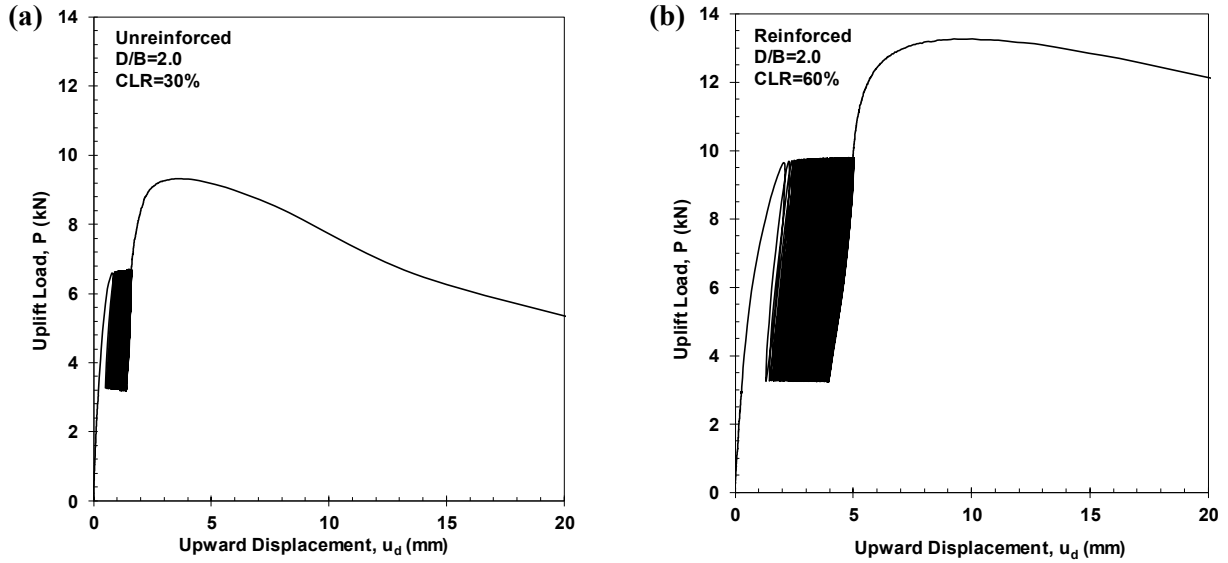


Fig. 18. Variation of the uplift load with anchor movement (a) unreinforced case, $D/B=2.0$ and $CLR=30\%$ (b) reinforced, $D/B=2.0$ and $CLR=60\%$.

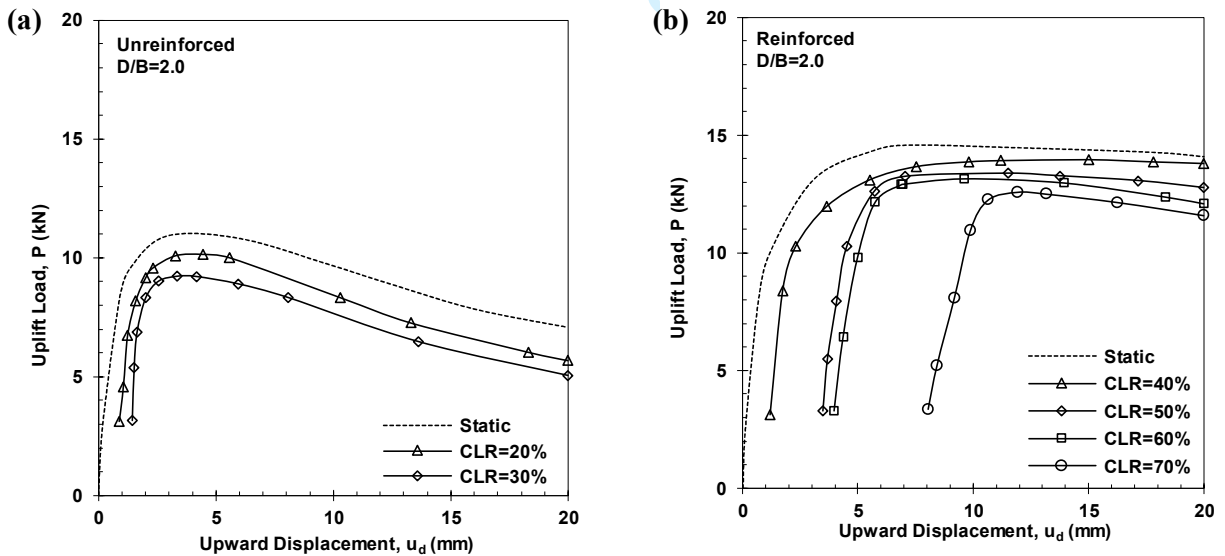


Fig. 19. Post-cycling behavior of anchor plate at $D/B=2$ and different cyclic load ratio, CLR (a) unreinforced case (b) reinforced case